

**GREEN SYNTHESIS, CHARACTERIZATION OF
ZINC OXIDE NANOPARTICLES AND THEIR
PHOTOCATALYTIC ACTIVITY**

WONG HONG LIANG

BACHELOR OF SCIENCE (HONS) CHEMISTRY

FACULTY OF SCIENCE

UNIVERSITI TUNKU ABDUL RAHMAN

MAY 2016

**GREEN SYNTHESIS, CHARACTERIZATION OF
ZINC OXIDE NANOPARTICLES AND THEIR
PHOTOCATALYTIC ACTIVITY**

By

WONG HONG LIANG

A project report submitted to the Department of Chemical Science,

Faculty of Science,

Universiti Tunku Abdul Rahman,

in partial fulfillment of the requirements for the degree of

Bachelor of Science (Hons) Chemistry

May 2016

ABSTRACT

GREEN SYNTHESIS, CHARACTERIZATION OF ZINC OXIDE NANOPARTICLES AND THEIR PHOTOCATALYTIC ACTIVITY

WONG HONG LIANG

Zinc oxide (ZnO) is a well-known *n*-type semiconductor with a band gap of 3.37 eV and excitation binding energy of 60 meV, hence consider as one of the best photocatalyst for degradation of pollutants in water. In order to enhance the photocatalytic activity of ZnO, nano-sized ZnO (ZnO NPs) have been synthesized to increase the surface area and enhance the photocatalytic activity. However, the synthesis of zinc oxide nanoparticles by conventional chemical methods always involves utilization of toxic chemical and expensive instruments along with the tedious process control. Therefore, it is a great demand for developing a simple, low cost and environmentally-friendly green method for synthesizing of ZnO NPs. In this study, synthesis of ZnO NPs using *Cavendish* banana peel extract (BP) as reducing agent and capping agent was reported. BP extract was prepared by boiling clean BP with deionized water for 10 minutes and filtered through filter paper twice. Then, BP extract was added dropwise into a pre-prepared zinc

acetate salt solution and stirred for 10 minutes on magnetic stirring hotplate. Zinc metal was precipitated out by adding in a base, 2M NaOH until the pH of the solution becomes pH 12 and finally, ZnO NPs was obtained through washing with water, filtration and dried in a 60°C oven. The synthesized ZnO NPs have been characterized using XRD, EDX, FTIR spectroscopy, UV-Vis spectroscopy, SEM and PSA. The photocatalytic activity of ZnO NPs has been investigated by degradation of Congo Red (CR) and Malachite Green (MG) dyes in aqueous solution with exposure to sunlight. The extent of dye degradation by ZnO NPs is monitored by using UV-Vis spectrophotometer.

ABSTRAK

SINTESIS, PENCIRIAN

DAN AKTIVITI FOTOKATALITIK

ZINK OKSIDA NANOPARTIKEL

WONG HONG LIANG

Zink oksida (ZnO) merupakan n-jenis semikonduktor yang terkenal dengan jurang jalur 3.37 eV dan tenaga ikatan teruja 60 MeV, oleh itu zink oksida dianggap sebagai salah satu fotokatalis yang terbaik untuk degradasi bahan pencemaran dalam air buangan. Untuk meningkatkan aktiviti fotokatalitik ZnO, ZnO yang bersaiz nano (ZnO NPs) telah disintesis untuk meningkatkan kawasan permukaan dan aktiviti fotokatalitik. Walau bagaimanapun, sintesis nanopartikel zink oksida yang diperolehi dengan kaedah kimia konvensional melibatkan penggunaan bahan kimia yang bertoksik dan kos instrumen yang mahal tambahan lagi dengan kawalan proses yang rumit. Oleh itu, pada masa kini terdapat permintaan yang besar untuk mensintesis ZnO NPs dengan cara yang lebih mudah, melibatkan kos rendah dan mengguna kaedah hijau mesra alam. Dalam kajian ini, sintesis ZnO NPs menggunakan *Cavendish* ekstrak kulit pisang (BP) sebagai agen penurunan dan agen penstabil dilaporkan. Ekstrak BP telah disediakan dengan

mendidih BP yang bersih dalam air ternaahion selama 10 menit dan ditapis melalui kertas penapis dua kali. Kemudian, ekstrak BP telah ditambah setitik-setitik ke dalam larutan zink asetat garam dengan proses pengacauan dijalankan selama 10 menit dengan magnet kacau plat panas. Logam zink dicetuskan dengan menambah dalam pangkalan, 2M NaOH sehingga pH penyelesaian menjadi pH 12 dan akhirnya, ZnO NPs dicuci dengan menggunakan air ternaahion beberapa kali, penapisan dan dikeringkan dalam ketuhar 60°C. Pencirian ZnO NPs yang disintesis dikenalpastikan dengan mengguna XRD, EDX, FTIR spektroskopi, spektroskopi ultra lembayung-cahaya nampak, SEM dan PSA. Aktiviti fotokatalitik ZnO NPs telah dikaji melalui degradasi Congo Red (CR) dan Malachite Green (MG) pewarna dalam larutan akueus dengan penyinaran cahaya matahari. Tahap degradasi pewarna oleh ZnO NPs dipantau dengan menggunakan spektrofotometer ultra lembayung-cahaya nampak.

ACKNOWLEDGEMENTS

First of all, I would like to express my sincere gratitude to Faculty of Science, Universiti Tunku Abdul Rahman (UTAR) for providing me such a great opportunity to explore on the research field. This opportunity has been provided me precious experience on how a basic research really looks like.

Next, I would like to express my deep appreciation to my final year project's supervisor, Dr. Mohammod Aminuzzaman for his enthusiasm, guidance and constant encouragement throughout the research period. His regular advice and suggestion made my work easier and proficient. I really appreciate the time he has taken to supervise me on skill and knowledge, thank you once again.

Furthermore, I am really feeling grateful to receive help from all laboratory officers from Faculty of Science (especially Mr. Ooh Keng Fei, Mr. Leong Thung Lim, Mr. Seou Chi Kien and Mr. Saravanan a/l Sivasangaran), Faculty of Engineering and Green Technology (Mr. Chin Kah Seng) and Dr. Ooi Mei Lee. They provided me a lot of useful techniques on handling equipment correctly as well as assisted me to run my synthesized product by using XRD, EDX, SEM, Particle Size Analyzer and LC-MS.

Last but not least, a special word of thanks also goes to my amazing family and friends (especially my lab partner, Ms. Leong Mei Kei) for their continuous and unconditional support, love and encouragement throughout the progress of this research.

DECLARATION

I hereby declare that the project report is based on my original work except for quotations and citations which have been duly acknowledged. I also declare that it has not been previously or concurrently submitted for any other degree at UTAR or other institutions.

WONG HONG LIANG

APPROVAL SHEET

I certify that, this project report entitled **“GREEN SYNTHESIS, CHARACTERIZATION OF ZINC OXIDE NANOPARTICLES AND THEIR PHOTOCATALYTIC ACTIVITY”** was prepared by WONG HONG LIANG and submitted as partial fulfillment of the requirements for the degree of Bachelor of Science (Hons) Chemistry at Universiti Tunku Abdul Rahman.

Approved by:

Date: _____

(Asst. Prof. Dr. Mohammad Aminuzzaman)

Supervisor

Department of Chemical Science

Faculty of Science

Universiti Tunku Abdul Rahman

FACULTY OF SCIENCE
UNIVERSITI TUNKU ABDUL RAHMAN

Date: _____

PERMISSION SHEET

It is hereby certified that **WONG HONG LIANG** (ID No: **12ADB03697**) has completed this thesis entitled “GREEN SYNTHESIS, CHARACTERIZATION OF ZINC OXIDE NANOPARTICLES AND THEIR PHOTOCATALYTIC ACTIVITY” under supervision of Asst. Prof. Dr. Mohammod Aminuzzaman from Department of Chemical Science, Faculty of Science.

I hereby give permission to the University to upload the softcopy of my thesis in pdf format into the UTAR Institutional Repository, which may be made accessible to the UTAR community and public.

Yours truly,

(WONG HONG LIANG)

TABLE OF CONTENTS

	Page
ABSTRACT	ii
ACKNOWLEDGEMENTS	vi
DECLARATION	vii
APPROVAL SHEET	viii
PERMISSION SHEET	ix
TABLE OF CONTENTS	x
LIST OF TABLES	xiii
LIST OF FIGURES	xiv
LIST OF ABBREVIATIONS	xix
 CHAPTER	
1 INTRODUCTION	1
1.1 Background of Study	1
1.2 Zinc Oxide Nanoparticles	2
1.2.1 Synthesis of Zinc Oxide Nanoparticles	4
1.3 Mechanism of Photocatalysis In Degradation of Dye	9
1.4 Objectives of Study	11
 2 LITERATURE REVIEW	 12

2.1	Green Synthesis of ZnO NPs	12
2.1.1	Synthesis Using Plant Extracts	13
2.1.2	Synthesis Using Agricultural Waste or Fruit Extracts	20
3	METHODOLOGY	28
3.1	Chemicals	28
3.2	Preparation of <i>Cavendish</i> Banana Peel (BP) Extract	28
3.3	Green Synthesis of Zinc Oxide Nanoparticles	30
3.4	Characterization of Synthesized Zinc Oxide Nanoparticles	32
3.5	Photocatalytic Activity of Synthesized Zinc Oxide Nanoparticles	36
3.5.1	Preparation of Dye Aqueous Solutions	36
3.5.2	Photocatalytic Dye Degradation	36
3.5.3	Determination of Percentage of Degradation	39
3.5.4	Identification of Degradation Products	39
4	RESULTS AND DISCUSSION	40
4.1	Green Synthesis of Zinc Oxide Nanoparticles	40
4.2	Characterization of Synthesized Zinc Oxide Nanoparticles	42
4.2.1	X-ray Diffraction (XRD)	42
4.2.2	Energy Dispersive X-ray Spectroscopy (EDX)	44

4.2.3	Fourier Transform Infrared Spectroscopy (FTIR)	46
4.2.4	Ultraviolet-Visible Spectroscopy (UV-Vis Spectroscopy)	48
4.2.5	Scanning Electron Microscope (SEM)	50
4.2.6	Particle Size Analyzer (PSA)	51
4.3	Evaluation of Photocatalytic Activity of Synthesized Zinc Oxide Nanoparticles	52
4.3.1	Degradation of Congo Red Dye in Aqueous Solution Using ZnO NPs under Solar Irradiation	53
4.3.2	Degradation of Malachite Green Dye in Aqueous Solution Using ZnO NPs under Solar Irradiation	56
4.3.3	Adsorption-Desorption and Photodegradation of Dye Aqueous Solution	59
4.3.4	Identification of Degradation Products for Malachite Green Dye Aqueous Solution by Liquid Chromatography-Mass Spectrometry	61
5	CONCLUSION	66
	REFERENCES	68
	APPENDICES	77

LIST OF TABLES

Table		Page
1.1	Conventional chemical synthesis methods for ZnO NPs	6
3.1	Time intervals for beakers to be collected during degradation process	37
4.1	EDX analysis processing data	44

LIST OF FIGURES

Figure		Page
1.1	Hexagonal-Wurzite structure of ZnO	2
1.2	Application of ZnO NPs	3
1.3	Synthetic methods for nanoparticles	4
1.4	Schematic diagram illustrated top-down and bottom-up synthesis	5
1.5	Schematic diagram for the uses of plant extract in nanoparticles synthesis	8
1.6	Chemical structure of dopamine and L-DOPA	8
1.7	Schematic diagram of photocatalysis degradation mechanism	9
2.1	<i>Ocimum tenuiflorum</i> plant	13
2.2	Characterization of ZnO NPs produced using <i>Ocimum tenuiflorum</i> plant extract - (A) XRD analysis and (B) SEM image	14
2.3	Overview of <i>Duranta erecta L.</i> plant	15
2.4	Various parts of <i>Duranta erecta L.</i> plant	15
2.5	Characterization of ZnO NPs produced using <i>Trifolium pratense</i> flower extract- (A) SEM image and EDX spectrum and (B) FTIR spectrum	16
2.6	Green tea leaves (A) Before and (B) After drying	17

2.7	Characterization of ZnO NPs produced using <i>Camellia sinesis</i> leaves extract - (A) Particle size analysis data, (B) SEM image and (C) UV-Vis spectrum	18
2.8	<i>Limonia acidissima</i> L. leaves	19
2.9	Characterization of ZnO NPs produced using <i>Limonia acidissima</i> L. leaves extract- (A) UV-Vis spectrum, (B) TEM image, (C) 2-D AFM topography and (D) 3-D AFM topography	19
2.10	<i>Poncirus trifoliata</i> or trifoliolate orange	21
2.11	Characterization of ZnO NPs produced using <i>Poncirus trifoliata</i> - (A) TEM image, (B) SEM image and (C) EDX spectrum	21
2.12	<i>Artocarpus gomezianus</i>	22
2.13	Characterization of ZnO NPs produced using <i>Artocarpus gomezianus</i> - (A) TEM image and (B) SEM image	22
2.14	3-D AFM topography of ZnO NPs produced using <i>Nephelium lappaceum</i> L. peel extracts	23
2.15	Proposed reaction mechanism for <i>Nephelium lappaceum</i> L. peel extract	24
2.16	(A) Plant of <i>Rosa canina</i> and (B) Ripped Fruit of <i>Rosa canina</i> , Rosehip	25

2.17	Characterization of ZnO NPs produced using <i>Rosa canina</i> fruit extract- (A) SEM image, (B) EDX spectrum and (C) Proposed reaction mechanism for <i>Rosa canina</i> fruit extracts	26
2.18	Characterization of ZnO NPs produced using lemon juice- (A) EDX spectrum and (B) SEM image	27
2.19	Proposed reaction mechanism for lemon juice	27
3.1	Process flowcharts for the preparation of <i>Cavendish</i> BP extract	29
3.2	Process flowcharts for the preparation of ZnO NPs using BP extract	31
3.3	Shimadzu XRD 6000	33
3.4	Perkin Elmer RX 1 FTIR Spectrometer	34
3.5	Perkin Elmer Lambda 35 UV-Visible Spectrophotometer	34
3.6	JEOL JSM-6701F SEM-EDX	35
3.7	Malvern Particle Size Mastersizer 2000	35
3.8	Process flowchart of photocatalytic dye degradation under solar irradiation	38
4.1	Photograph of ZnO NPs synthesized using <i>Cavendish</i> BP extract	40
4.2	XRD Diffractogram of Synthesized ZnO NPs	42
4.3	EDX spectrum of synthesized ZnO NPs	44

4.4	FTIR spectra of synthesized ZnO NPs with BP extract	46
4.5	UV-Visible spectrum of synthesized ZnO NPs	48
4.6	SEM images of synthesized ZnO NPs at different magnifications	50
4.7	Particle size analysis spectrum with processing data	51
4.8	UV-Vis spectrum of CR dye degradation as a function of contact time (minutes)	53
4.9	Photograph of degraded CR dye aqueous solution in different time interval	53
4.10	Chemical structure of CR dye	54
4.11	Degradation percentage of CR as a function of time	54
4.12	UV-Vis spectrum of MG dye degradation as a function of contact time (minutes)	56
4.13	Photograph of degraded MG dye aqueous solution in different time intervals	56
4.14	Chemical structure of MG dye	57
4.15	Degradation percentage of MG as a function of time	57
4.16	Mass spectra of (A) 4-hydroxybenzoic acid, (B) 4-(dimethylamino)-benzophenone, (C) didesmethyl MG, (D) desmethyl MG, (E) MG, (F) Leuco MG and (G) MG leucocarinol	61

4.17 Tentative degradation pathway of MG dye in aqueous
solution using ZnO NPs

64

LIST OF ABBREVIATIONS

2-D	Two dimensional
3-D	Three dimensional
A	Ampere or absorbance
Å	Angstrom
A ₀	Initial absorbance of dye solutions
A _i	Absorbance of dye solutions at a given contact time
AA	Ascorbic acid
AFM	Atomic Force Microscope
Al	Aluminum
BP	Banana peel
C	Carbon
c	Speed of light
Ca	Calcium
CB	Conduction band
cm ⁻¹	Frequency unit or wavenumber
CO ₂	Carbon dioxide
CR	Congo Red
E _{bg}	Band gap energy
EDX	Energy Dispersive X-ray

eV	Electronvolt
e ⁻	Electron
FTIR	Fourier Transform Infrared
FWHM	Full width half maximum
g	Gram
GC-MS	Gas chromatography-mass spectrometry
h	Planck's constant
HO [·]	Hydroxyl radical
HO ₂ [·]	Hydroperoxyl radical
<i>hν</i>	Light
H ₂ O	Water molecule
H ₂ O ₂	Hydrogen peroxide
JCPDS	Joint Committee on Powder Diffraction Standards
k	Sherrer constant
KBr	Potassium bromide
kV	Kilovolt
L	Liter
LC-MS	Liquid chromatography-mass spectrometry
M	Mega or molar concentration
m	Milli
MB	Methylene Blue

MG	Malachite Green
Mg	Magnesium
MO	Methyl Orange
MR	Methyl Red
MS	Mass spectrum
NaOH	Sodium hydroxide
nm	Nanometer
O	Oxygen
OH ⁻	Hydroxide ion
OM	Organic molecules
O ₂	Oxygen
O ₂ ⁻	Superoxide
PEG	Polyethylene glycol
pH	Potential of hydrogen
pH _{zpc}	pH point of zero charge
ppm	Part per million
PSA	Particle Size Analyzer
Q-TOF	Quadrupole-Time-Of-Flight
rpm	Revolution per minute
SDS	Sodium dodecyl sulphate
SEM	Scanning Electron Microscope

TEM	Transmission Electron Microscope
TiO ₂	Titanium (IV) dioxide
UV	Ultraviolet
UV-Vis	Ultraviolet-Visible
VB	Valence band
VOC	Volatile organic solvent
W	Waltz
XRD	X-ray Diffraction
ZnO	Zinc oxide
ZnO NPs	Zinc oxide nanoparticles
Zn(0)	Zinc(0)
Zn(II)	Zinc(II)
Zn(OH) ₂	Zinc hydroxide
λ	Wavelength of X-ray source or lambda
λ_{\max}	Lambda maximum
°C	Degree Celsius
θ	Bragg's diffraction angle
β	Full width at half-maximum of the diffraction peak
π	Pi
μ	Micro

CHAPTER 1

INTRODUCTION

1.1 Background of Study

Nanotechnology is being widely applied in the field of material science in the past decades. This concept was first attempted in an American physicist, Richard Feynman's lecture in 1959 (Kavitha et al., 2013). Nanotechnology is dealing with the production of materials in a nanometer scale level, normally from 1 to 100 nanometers (nm) such as carbon nanotube (Martel et al., 1998), metal nanowire (Penner et al., 2003) with unique electrical and mechanical properties and nanoparticles. Nanoparticles are of great interest due to their small size and large surface area to volume ratio (Poinern et al., 2015) that give rise to some of the superior properties than their bulk phase such as antimicrobial, catalytic, electronic, magnetic and optical properties (Shah et al., 2015)

1.2 Zinc Oxide Nanoparticles

Metal and metal oxide nanoparticles such as titanium (IV) dioxide (TiO_2) and zinc oxide (ZnO) have been extensively studied by many researchers due to their good stability toward harsh process conditions (Ramesh et al., 2014). Zinc oxide nanoparticles (ZnO NPs) are one of the metal oxide nanoparticles which are non-toxic, insoluble in water with density of 5.606 g cm^{-3} and appear as a white powder with refractive index of 2.0041. It also possesses a high boiling and melting points which are 2360°C and 1975°C respectively. The crystal structure of ZnO is in hexagonal-wurtzite shown in Figure 1.1 where oxygen atoms (white spheres) are tetrahedral coordinated to Zn atom (black spheres).

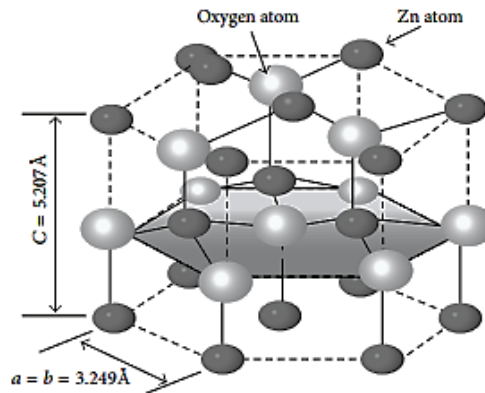


Figure 1.1: Hexagonal-Wurtzite structure of ZnO (Sabir et al., 2014)

The most attractive factor in using ZnO NPs is that it has versatile application where some of them are shown in Figure 1.2.

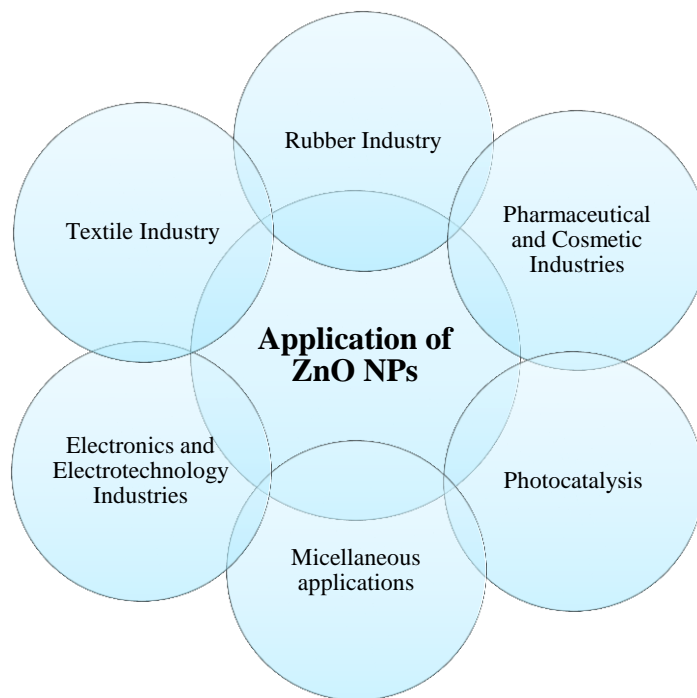


Figure 1.2: Application of ZnO NPs (Kolodziejczak-Radzimska et al., 2014; Oudhia et al., 2015 and Gnanasangeetha and Thambavani, 2014)

ZnO NPs is a semiconductor with wide band gap energy of 3.37 eV and large excitation binding energy of 60 MeV. (Varghese and George, 2015). The similarity of semiconductor properties between ZnO NPs and the well-known photocatalyst system in the degradation of organic dyes, TiO₂ NPs with 3.2 eV band gap energy (Giwa et al., 2012) makes it another powerful photocatalyst possible in the degradation of dyes.

1.2.1 Synthesis of Zinc Oxide Nanoparticles

There are various synthetic methods have been reported by researchers to synthesize nanoparticles mainly divided into three classes shown in Figure 1.3.

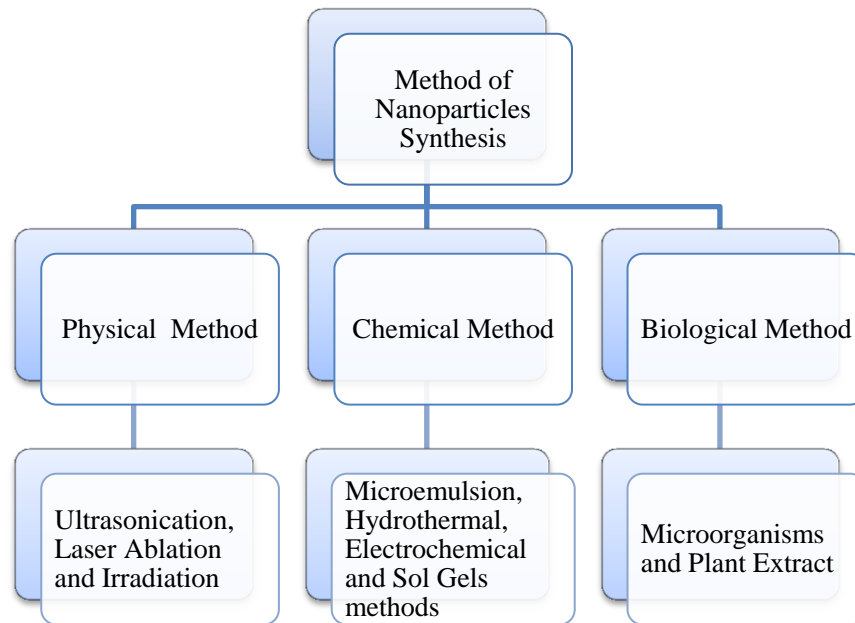


Figure 1.3: Synthetic methods for nanoparticles (Kumar et al., 2015)

Nanoparticles can be obtained via either top-down or bottom-up processes shown in Figure 1.4. Top-down process also called physical methods involved the breaking down of bulk into small using mechanical energy such as lithography whereas bottom-up process also called chemical methods involved the joining atom by atom forming nano-sized particles (Saravanan et al., 2008).

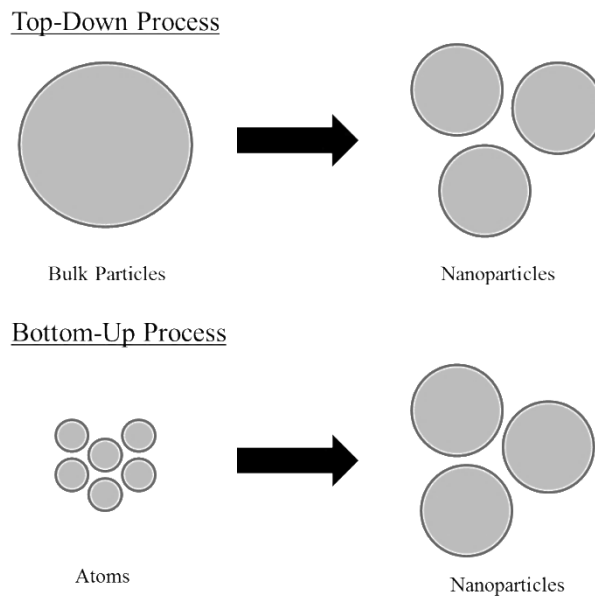


Figure 1.4: Schematic diagram illustrated top-down and bottom-up synthesis

In order to obtain a desired size, shape, stability and physiochemical properties of synthesized nanoparticles, the reaction conditions must be properly designed in some factors such as the temperature and pressure control, and the requirement of the reducing agent (reduction of metal ion) and stabilizing agent (restrict nanoparticles from agglomeration) towards the metal ion precursor (Shamsuzzaman et al., 2014). In the conventional synthetic method, both physical and chemical often required reducing agent and stabilizing agent that are non-benign and highly toxic to the surrounding environment. Besides, these methods are also costly, high energy consumption and the high possibility for the formation of toxic by-product (Senthilkumar and Sivakumar, 2014). A list of chemical synthesis method in details was shown in Table 1.1.

Table 1.1: Conventional chemical synthesis methods for ZnO NPs (Kolodziejczak-Radzimska et al., 2014)

Chemical Methods	Precursors	Reaction Conditions
Precipitation with surfactants	Zinc nitrate, NaOH, SDS and triethanolamine	Temperature: 101°C Duration: 50-55 minutes
Sol-Gel Method	Zinc acetate, oxalic acid, ethanol and methanol	Temperature: 60°C Drying: 80°C for 24 h Calcination: 500°C
Hydrothermal Method	Zinc chloride, NaOH	Temperature: 100-220°C Duration: 5-10 h Equipment: Teflon-lined autoclave
Microemulsion	Zinc nitrate, NaOH, heptane, hexanol, Triton X-100, PEG-400	Temperature: 140°C Duration: 15 h Drying: 60°C

However, these problems can be effectively reduced through a greener approach in using the biological method production. This method employs the use of microorganisms such as bacteria and fungi or plant extract. Plant extract has been reported to be more advantageous over the microbes as it does not required high cost of isolation, cultivation and maintenance, high yield can be obtained in a short period of time for industrial scale consideration and etc. (Shamsuzzaman et al., 2014).

Plant extract is used as a potential substitute for the reducing agent and stabilizing agent due to the combination of its bio-components such as alkaloids, terpenoids, tannins, phenolics, amino acids, proteins, enzymes, polysaccharides, saponins, vitamins and etc. (Ahmed et al., 2016). Besides, various fruits peel extracts are of great interest because somehow they are having the similar properties to the plant extract as certain fruit peels are also rich in these bio-components and easily available. Meanwhile, it is a very good practice in the sense of fully utilizing the waste created and reduces their impacts to the environment that highly fulfilled the green chemistry aspect. On the basis of reported information, banana peel extract is one of the potential materials available for the synthesis of nanoparticles because it contained a huge amount of dopamine and L-DOPA as well as other bio-components that serve as the reducing agent and macromolecules such as lignins, pectins, and hemicellulose with stabilizing properties (Kokila et al., 2015). Dopamine and L-DOPA are catecholamine with high antioxidant activity due to the presence of catechol functional group (Gonzalez-Montelongo et al., 2010; Jodko-Piorecka et al., 2015).

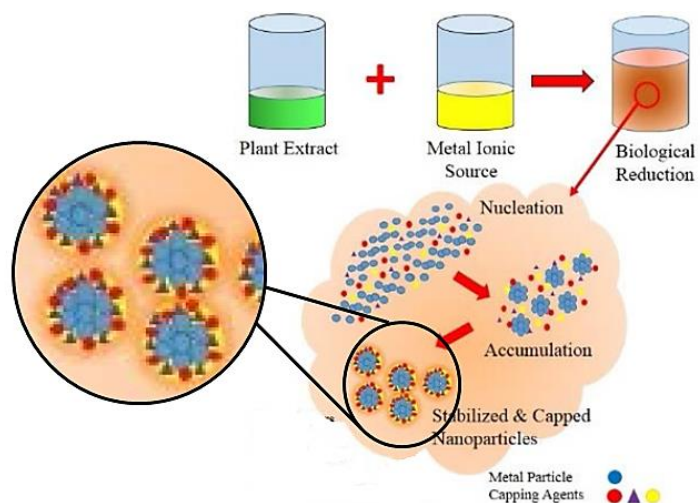


Figure 1.5: Schematic diagram for the uses of plant extract in nanoparticles synthesis (Poinern et al., 2015)

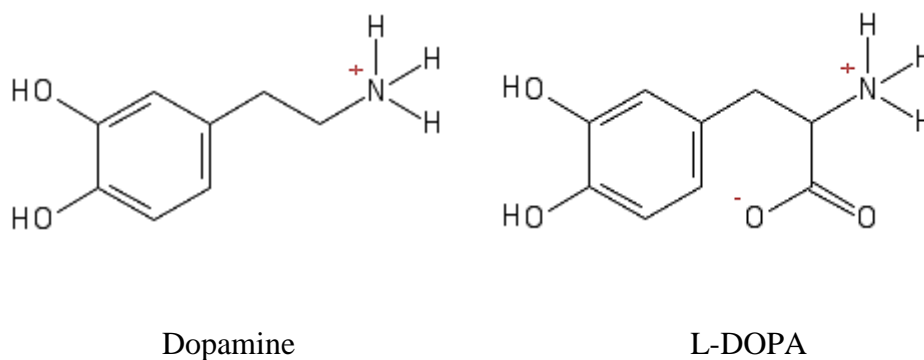


Figure 1.6: Chemical structure of dopamine and L-DOPA (Jodko-Piorecka et al., 2015)

1.3 Mechanism of Photocatalysis In Degradation of Dye

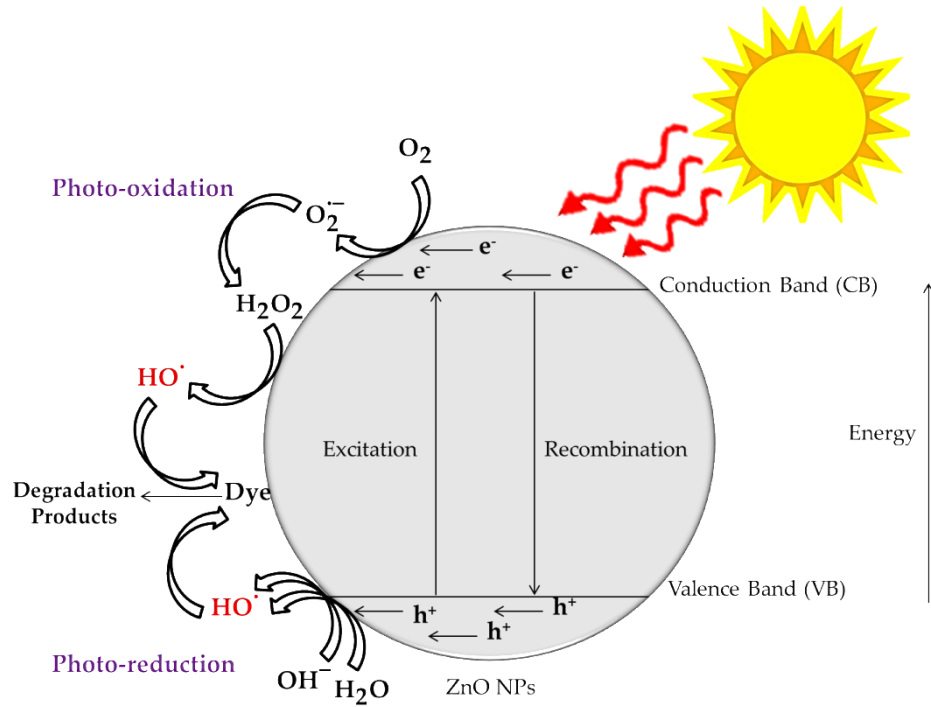
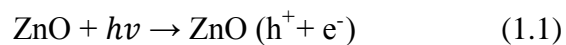
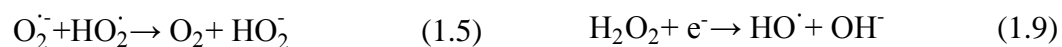


Figure 1.7: Schematic diagram of photocatalysis degradation mechanism (Giwa et al., 2012)

Figure 1.7 shows the mechanism of photocatalysis where a series of reaction occurred on the surface of ZnO NPs. Photocatalysis is first initiated by placing ZnO NPs suspension under natural sunlight, an electron (e^-) will be promoted from the valence band (VB) to the conduction band (CB) of semiconductor through absorbing energy from UV-light generates an excited electron and a hole shown in (1.1).



This pair of electron and hole can be either recombine with each other or initiates a series of photo-oxidation and photo-reduction reactions with oxygen on the surface of the ZnO NPs semiconductor shown in (1.2) to (1.9).



(Curri et al., 2003; Giwa et al., 2012)

In the solution, hole generated oxidizes the hydroxide ion (OH^-) and water (H_2O) forming hydroxyl radical shown in (1.10) to (1.11). These reactions resulted in the formation of a very powerful oxidizing agent, hydroxyl radical ($\text{HO} \cdot$) which is the species responsible to complete the mineralization of dye molecules (OM) into end product carbon dioxide (CO_2) and water (H_2O) if time permitted (1.12).



(Curri et al., 2003; Giwa et al., 2012)

1.4 Objectives of Study

1. To synthesize ZnO NPs through a green synthetic pathway using *Cavendish* banana peel extract.
2. To characterize synthesized ZnO NPs using Fourier Transform Infrared (FTIR) Spectroscopy, Ultraviolet-Visible (UV-Vis) Spectroscopy, Energy Dispersive X-ray Spectroscopy (EDX), Scanning Electron Microscope (SEM), X-ray Diffraction (XRD) and Particle Size Analyzer (PSA).
3. To evaluate the photocatalytic activity of the synthesized ZnO NPs by degradation of diazo dye, Congo Red (CR) and cationic dye, Malachite Green (MG) in aqueous solution with exposure to natural sunlight. The extent of dye degradation by ZnO NPs is monitored by using UV-Vis spectrophotometer. Preliminary screening of the intermediate products as well as the photocatalytic degradation pathway of MG are analyzed, identified and proposed using Liquid Chromatography-Mass Spectrometry (LC-MS).

CHAPTER 2

LITERATURE REVIEW

2.1 Green Synthesis of ZnO NPs

The usefulness of nanoparticles is so attractive that bulk synthesis often required. Researchers nowadays are more preferred to synthesize nanoparticles using plant, agricultural waste and fruit extract to minimize the uses of toxic chemicals and harsh reaction conditions that consequently contribute significant risk to the environment. In this literature review, ZnO NPs synthesized using green methods are listed into two categories which are plant extracts (*Duranta erecta L.*, *Ocimum tenuiflorum*, *Camellia sinesis*, *Limonia acidissima L.*, and *Trifolium pretense*) and agricultural waste and fruit extracts (Rambutan peel, lemon juice, *Artocarpus gomezianus*, trifoliolate orange and *Rosa canina* fruit) that has been studied by other researchers.

2.1.1 Synthesis Using Plant Extracts

A member of Lamiaceae family, *Ocimum tenuiflorum* plant leaves extract of was used by Raut et al., (2013) to synthesize ZnO NPs. The authors reported that a mixture of *Ocimum tenuiflorum* plant extract and zinc nitrate solution was stirred together forms a light yellow color ZnO NPs with an average crystalline size of 13.86 nm and 11-25 nm hexagonal particle diameters from XRD analysis and SEM image shown in Figure 2.2. The presence of bio-components, mainly alkaloids, tannins, glycosides, ursolic acid flavonoids etc. (Joshi et al., 2010; Devendran et al., 2011; Aqil et al., 2006) on the surface of nanoparticles was observed through the FTIR analysis where hydroxyl, amine, alkyl halide and etc. bond vibrational bands were found in the spectrum. The formation of ZnO NPs was confirmed by observing the Zn-O bond vibration in fingerprint region of the spectrum.



Figure 2.1: *Ocimum tenuiflorum* plant (Raut et al., 2013)

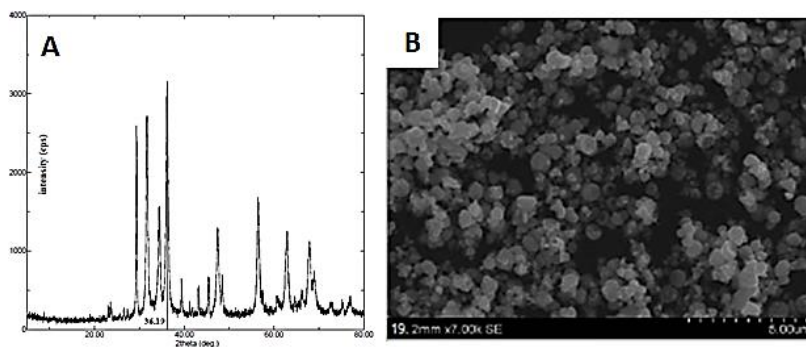


Figure 2.2: Characterization of ZnO NPs produced using *Ocimum tenuiflorum* plant extract- (A) XRD analysis and (B) SEM image (Raut et al., 2013)

Shekhawat et al., (2016) reported the uses of fruits, leaves, flowers, stems and roots of a Verbenaceae family member often found in tropical and subtropical country around the world which normally used for decoration, *Duranta erecta L.* plant to synthesize ZnO NPs and characterized using UV-Vis spectroscopy. Previous study was done by other researchers verified that it contains some phytoconstituents in methanolic extract such as polyphenols (tannins and flavonoids), saponins, alkaloids and glycosides (Ahmed et al., 2009; Khanal et al., 2014; Sharma et al., 2012). It possesses the antioxidant properties due to the presence of flavonoids, alkaloids, tannins and etc. By referring to the UV-Vis spectra obtained, each part of the plant extract given the different values of λ_{\max} under the Ultraviolet (UV) region which are 293 nm for roots, 299 nm for flowers and stems, 302 nm for leaves and 317 nm for fruits. These values of λ_{\max} in the range of 290 nm – 320 nm are the characteristic absorption peaks from ZnO NPs.



Figure 2.3: Overview of *Duranta erecta L.* plant (Shekhawat et al., 2016)

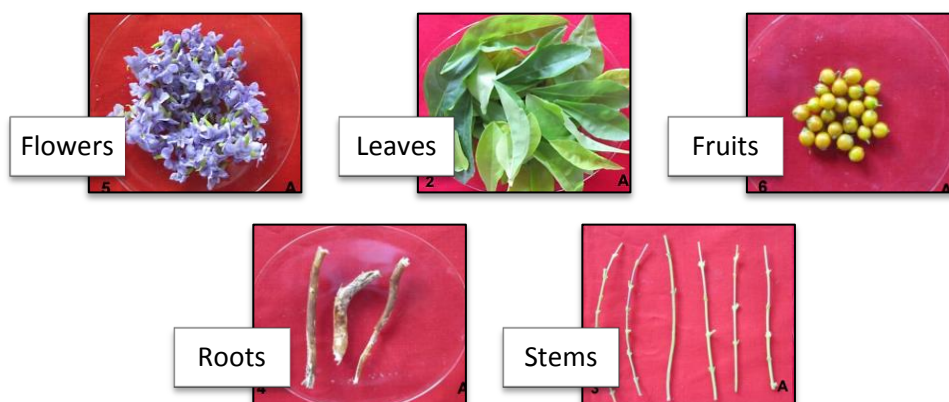


Figure 2.4: Various parts of *Duranta erecta L.* plant (Shekhawat et al., 2016)

Green synthesis of 60 to 70 nm crystalline size and 190 nm particle size ZnO NPs in high purity was found to be useful using red clover, *Trifolium pratense* flower extract, a member of Leguminosae family (Dobrucka et al., 2015). Synthesized ZnO NPs in this method was characterized by authors using SEM-EDX, XRD, FTIR, UV-Vis spectrophotometry and studied its antimicrobial ability towards five selected microorganisms. The reported bio-components in *Trifolium pratense*

were major in estrogenic isoflavones and flavonoids such as biochanin A-G-M, formononetin-G-M and quercetin-G-M (Klejdus et al., 2001; Saviranta et al., 2010) that are responsible for reducing and stabilizing purpose. Characterization results were shown in Figure 2.5. FTIR analysis revealed some important vibrational bands such as hydroxyl group, C-O, Zn-O etc. that correspond to the ZnO NPs and also the bio-compounds that present on its surface. The λ_{\max} belongs to ZnO NPs in UV-Vis spectrum was measured at 283 nm using double distilled water as blank.

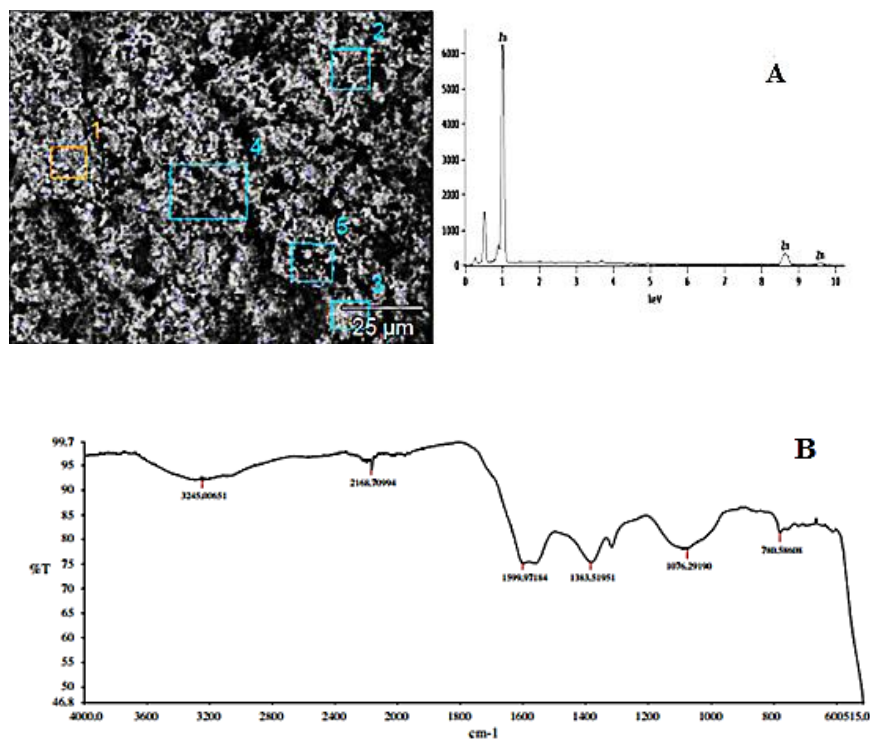


Figure 2.5: Characterization of ZnO NPs produced using *Trifolium pratense* flower extract- (A) SEM image and EDX spectrum and (B) FTIR spectrum (Dobrucka et al., 2015)

A very common antioxidant, green tea, *Camellia sinensis* leaves extract was also used to synthesize ZnO NPs and studied its antimicrobial activity on certain selected microbes (Shah et al., 2015; Senthilkumar et al., 2014). Characterization results were shown in Figure 2.7. The reported average crystalline size and particle size of synthesized ZnO NPs were 16 nm and 853 nm respectively, signal generated from XRD analysis and PSA with a number of aggregates observed in SEM images. Besides, the presence of the λ_{\max} in spectrum of UV region at 325 nm to 330 nm corresponds to the absorption from ZnO NPs. FTIR spectrum showed some significant bands such as hydroxyl group, amine, carbonyl, and aromatic stretching produced by the polyphenols, amino acids, proteins and other bio-components. According to the authors, these *Camellia sinensis* leaves extract induced synthesis of ZnO NPs possesses a very good antimicrobial activity towards the bacteria (Gram positive and Gram negative) and fungal strains as compared with a positive control.



Figure 2.6: Green tea leaves (A) Before and (B) After drying (Senthilkumar et al., 2014)

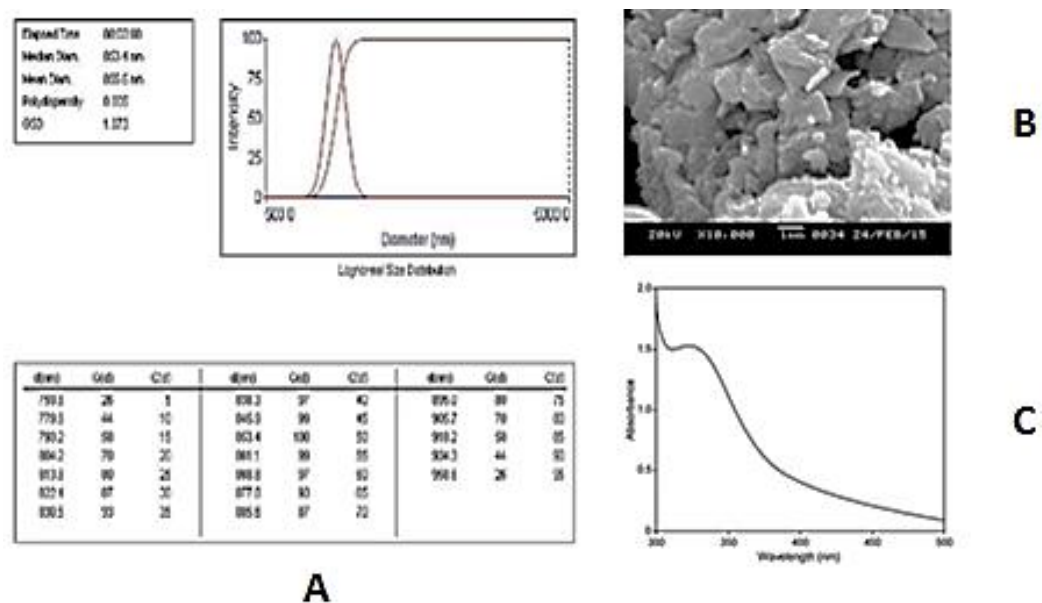


Figure 2.7: Characterization of ZnO NPs produced using *Camellia sinensis* leaves extract- (A) Particle size analysis data, (B) SEM image and (C) UV-Vis spectrum (Shah et al., 2015)

Spherical ZnO NPs in particle size range of 12-53 nm was produced using extract of a member from Rutaceae family mostly found in India, *Limonia acidissima* L. leaves with zinc nitrate solution precursor (Bheemanagouda et al., 2016). Phytochemical analysis of *Limonia acidissima* L. leaves extract shows high amount of flavonoids and tannins, compounds that give high antioxidant properties (Pandavadra et al., 2014). According to the authors, the synthesized ZnO NPs was characterized using FTIR and UV-Vis spectrophotometry whereas size and morphology was analyzed using TEM, AFM and XRD. Characterization results were shown in Figure 2.9. Functional group vibrational bands shown in FTIR spectrum confirmed the presence of phenolic compounds and proteins

(macromolecules) that covered on the nanoparticles together with characteristic Zn-O band. The maximum absorption of the synthesized ZnO NPs was found at 378 nm in UV region of spectrum.



Figure 2.8: *Limonia acidissima* L. leaves (Pandavadra et al., 2014)

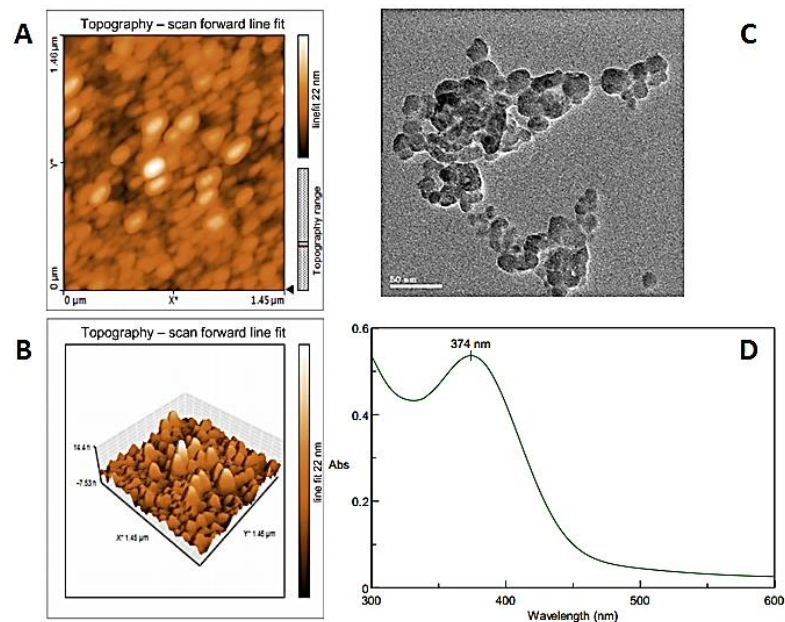


Figure 2.9: Characterization of ZnO NPs produced using *Limonia acidissima* L. leaves extract- (A) UV-Vis spectrum, (B) TEM image, (C) 2-D AFM topography and (D) 3-D AFM topography (Bheemanagouda et al., 2016)

2.1.2 Synthesis Using Agricultural Waste or Fruit Extracts

Synthesis of ZnO NPs using another member from Rutaceae family, *Poncirus trifoliata* fruits extract, trifoliata orange was done by Nagajyothi et al., (2013) and their catalytic activity in Claisen Schmidt condensation reaction between acetophenone and 3,4-dimethylbenzaldehyde was evaluated. According to Nogata et al., (2006), *Poncirus trifoliata* fruits extract was found to be contains large amount of flavonoids, including flavanone, flavone and polymethoxylated flavone that participating in the reduction of zinc ion during the synthesis of ZnO NPs due to their excellent antioxidant ability. Characterization results were shown in Figure 2.11. The spherical particle sizes obtained were 21.12 nm in average according to SEM and TEM images, UV-Vis spectrum, XRD and EDX analysis confirmed the identity of the synthesized ZnO NPs and also FTIR analysis verified the presence of bio-components coated on the surface of NPs by observing certain functional group vibrational modes in the spectrum such as alcohol, phenol, aromatic and 1° amine.



Figure 2.10: *Poncirus trifoliata* or trifoliolate orange (Hardy, 2004)

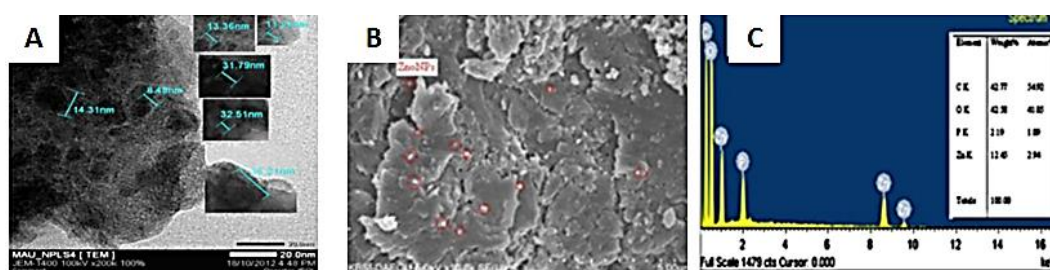


Figure 2.11: Characterization of ZnO NPs produced using *Poncirus trifoliata*- (A) TEM image, (B) SEM image and (C) EDX spectrum (Nagajyothi et al., 2013)

Artocarpus gomezianus extract assisted synthesis of ZnO NPs and their photocatalytic ability evaluation on Methylene Blue (MB) organic dye degradation was done by Suresh et al., (2015). *Artocarpus gomezianus* belongs to *Artocarpus* family that normally found in Central Western Ghats which are rich in flavonoids, stilbenoids, arylbenzofurans and Jacalin (Jagtap et al., 2010). However, according to the phytochemical studies done by Krishnamurthy et al., (2013), *Artocarpus gomezianus* fruit extract is richest in alkaloids and poor in steroids. Suresh et al., (2015) reported there is 17.16% polyphenol and 22% of flavonoids in *Artocarpus gomezianus* fruit extract. These secondary metabolites

were useful in the reduction of zinc ion that leads to the formation of ZnO NPs. The authors characterized the synthesized NPs using XRD and UV-Vis spectrophotometry and studied their surface morphology using SEM and TEM. Characterization results were shown in Figure 2.13. The crystalline size obtained from this methodology is 11.53 nm in spherical shape. MB was effectively removed by this synthesized ZnO NPs where > 90% MB can be degraded under the natural sunlight irradiation.



Figure 2.12: *Artocarpus gomezianus* (Suresh et al., 2015)

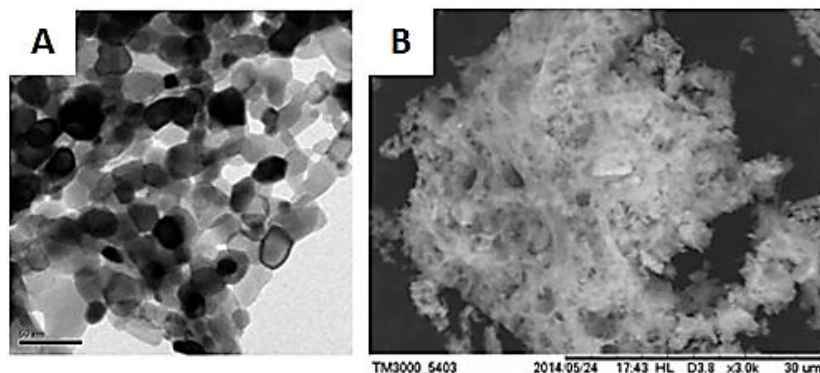


Figure 2.13: Characterization of ZnO NPs produced using *Artocarpus gomezianus*- (A) TEM image and (B) SEM image (Suresh et al., 2015)

Rambutan, *Nephelium lappaceum* L. peel was another choice of agricultural waste can be used to prepare extract as it contains powerful antioxidant (Thitilertdecha et al., 2008). Yuvakkumar et al., (2014) used the *Nephelium lappaceum* L. peel extract with zinc nitrate to synthesize ZnO NPs through the formation of Zinc ellagate complex intermediate with some polyphenols such as ellagic acid. It is capable to act as a ligand that binds to the zinc metal ion and decomposes to ZnO NPs after calcination. The proposed reaction mechanism of *Nephelium lappaceum* L. peel extract with zinc metal ion is shown in Figure 2.15. The crystalline and particles sizes were found to be 50.95 nm and 450 nm with agglomerates respectively. From the AFM topography, 3-D image clearly displayed a smooth and needle-like agglomerated ZnO NPs as shown in Figure 2.14. FTIR spectrum given the information of Zn-O stretching as well as O-H stretching arises from polyphenol compounds.

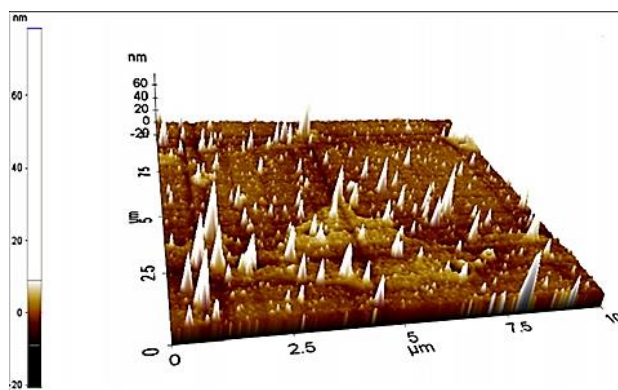


Figure 2.14: 3-D AFM topography of ZnO NPs produced using *Nephelium lappaceum* L. peel extract (Yuvakkumar et al., 2014)

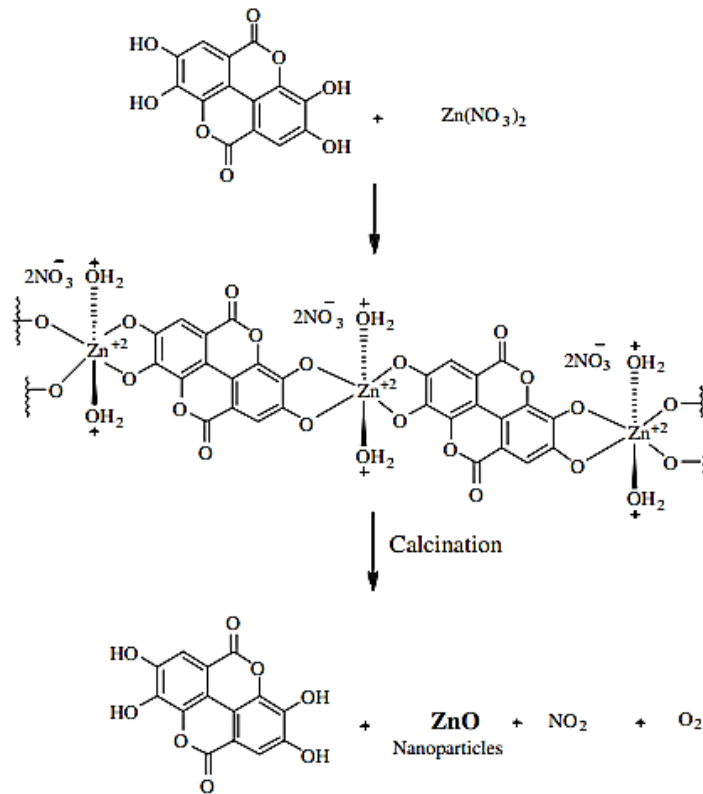


Figure 2.15: Proposed reaction mechanism for *Nephelium lappaceum* L. peel extract (Yuvakkumar et al., 2014)

Demir et al., 2014 reported that a member from *Rosaceae* family, *Rosa canina* fruit, rosehip extract possesses high antioxidant activity due to the presence of phenolic acids such as gallic acid, flavonoids such as catechin, proanthocyanidin such as procyanidin B2, sugars and organic acids such as ascorbic acid (AA or vitamin C). Based on these analysis data, Jafarirad et al., (2016) used the same concept as Thitilertdecha et al., (2008) produced ZnO NPs with the stabilizing activity from the chelation of AA to the zinc ion through its polar hydroxyl functional group. The reaction mechanism is shown in Figure 2.17 (C). Spherical ZnO NPs with crystalline and particle sizes synthesized from microwave irradiation were 11.3 nm and < 50 nm respectively. EDX data shown in Figure 2.17 (B) confirmed the high purity of synthesized ZnO NPs where the weight percent of Zn gives 65.19% and oxygen gives 34.81%. FTIR spectrum reveals the presence of AA on the surface of ZnO NPs from the detected bond vibrations such as C=O, C-O stretch of ester, C-H, O-H stretch as well as Zn-O stretches.

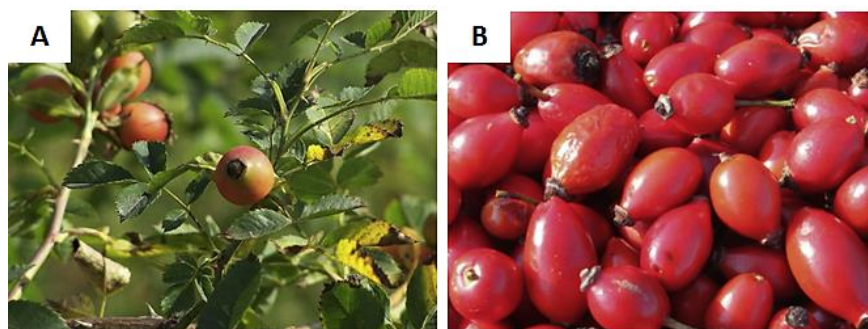


Figure 2.16: (A) Plant of *Rosa canina* and (B) Ripped Fruit of *Rosa canina*, Rosehip (Ahmad et al., 2016)

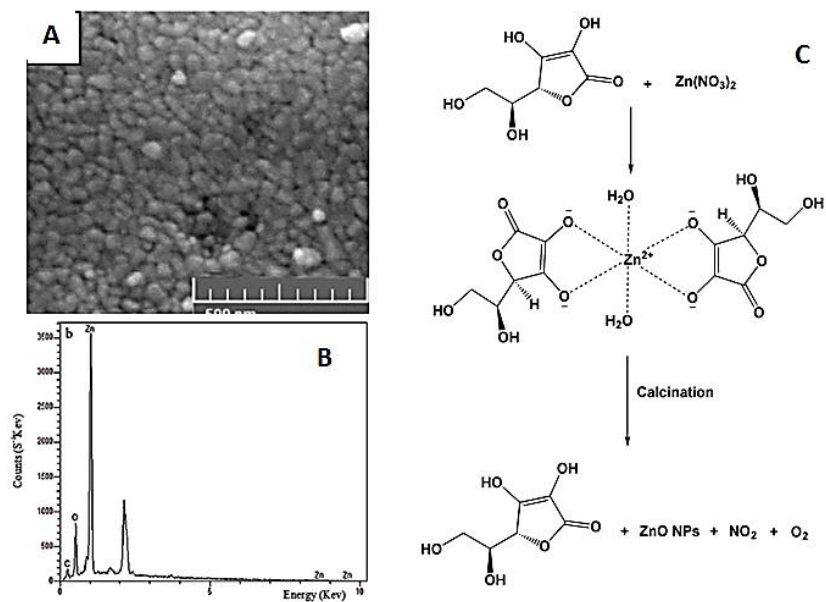


Figure 2.17: Characterization of ZnO NPs produced using *Rosa canina* fruit extract- (A) SEM image, (B) EDX spectrum and (C) Proposed reaction mechanism for *Rosa canina* fruit extract (Jafarirad et al., 2016)

Lemon juice is rich in citric acid, which acts as a chelating agent in forming a stable complex with zinc ion precursor, with the aids of added sucrose in the synthesis of ZnO NPs in ethylene glycol solvent (Davar et al., 2015). Sucrose in lemon juice readily undergoes hydrolysis into glucose and fructose which in turns oxidized to carboxylic group containing compounds such as saccharic acid that chelate to zinc ion like citric acid. The purpose of using this method was to obtain a more uniform particle distribution ZnO NPs. This effort was confirmed by observing the SEM images shown in Figure 2.18 (B). EDX results in Figure 2.18 (A) showing peaks for Calcium (Ca) and Magnesium (Mg) come from lemon juice (Lorente et al., 2014) and also the Zn and O from nanoparticles. Then, the

photocatalytic activity of synthesized ZnO NPs was evaluated on degradation of methyl orange (MO), methyl red (MR), MB organic and reactive blue 21 textile dyes. MO shows almost 100% degradation efficiency while MR and MB show only up to 60% after 35 minutes degradation. Reactive blue 21 shows more than 75% degraded after 4 hours 30 minutes irradiation.

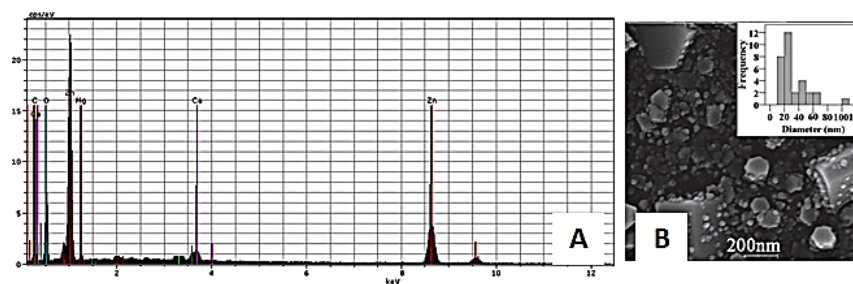


Figure 2.18: Characterization of ZnO NPs produced using lemon juice- (A) EDX spectrum and (B) SEM image (Davar et al., 2015)

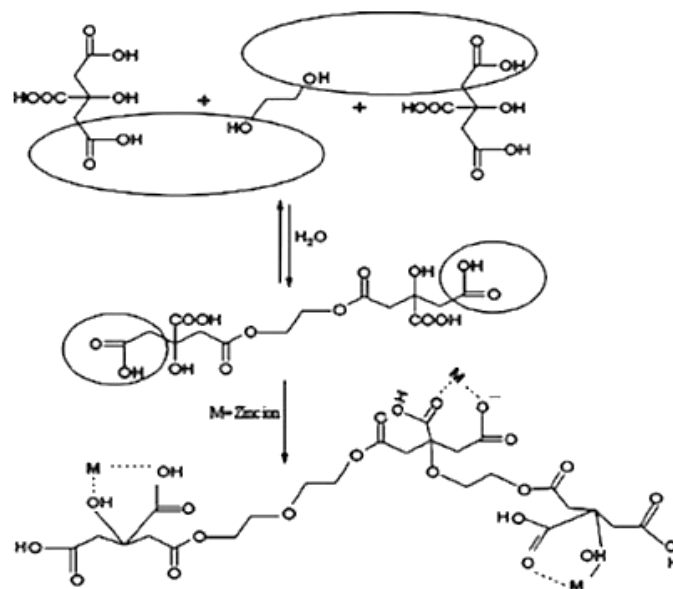


Figure 2.19: Proposed reaction mechanism for lemon juice (Davar et al., 2015)

CHAPTER 3

METHODOLOGY

3.1 Chemicals

Cavendish banana was purchased from Tesco Kampar, Perak, Malaysia. Sodium hydroxide (NaOH) pellets was purchased from Sigma-Aldrich together with deionized water that used in the preparation of extract. Zinc acetate dihydrate salt precursor was purchased from MERCK. Congo Red and Malachite Green dyes were obtained from R&M Chemicals and QRec (Quality Reagent Chemical Product) respectively. All glasswares were properly cleaned with deionized water and dried in an oven before use.

3.2 Preparation of *Cavendish* Banana Peel (BP) Extract

Cavendish BP was washed repeatedly with deionized water to remove particulate matter and other impurities on it. Then, the peels were dried on paper toweling and cut into pieces. About 50 g of peels were weighed and added into 250 mL beaker containing 50 mL of deionized water and boiled in 80° C for 10 minutes.

The weight of peels and volume of deionized water used can be varied as long as it remains in the ratio of 1:1. Finally, the peel extract was cooled down and filtered through Whatman No.1 filter paper twice on filter funnel. The resulting filtrate was directly used in the next step of the synthesis part.

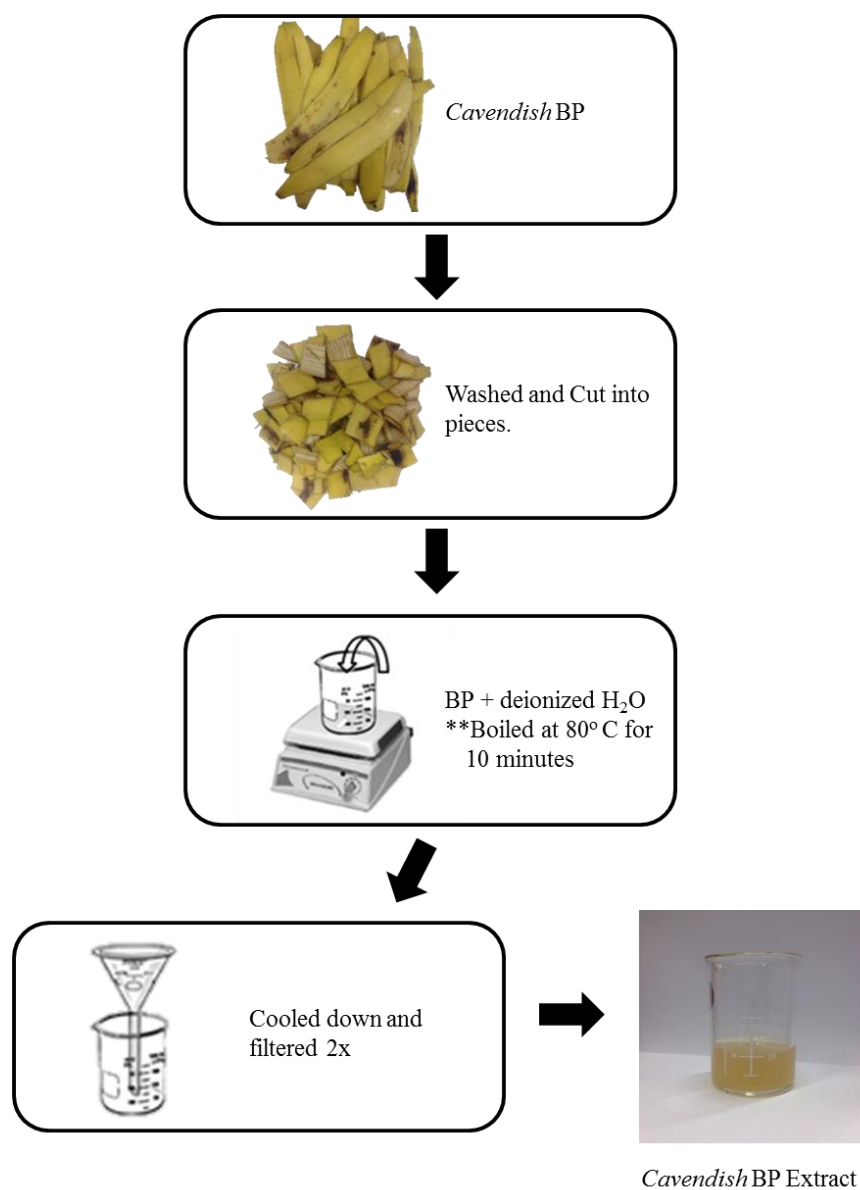


Figure 3.1 Process flowcharts for the preparation of *Cavendish* BP extract

3.3 Green Synthesis of Zinc Oxide Nanoparticles

About 0.25 g of zinc acetate dihydrate was stirred to dissolve in a 250 mL beaker containing 50 mL of deionized water. Then, 4 mL of BP extract prepared in Section 3.2 was added dropwise and stirred on a magnetic stirring hotplate with magnetic stirrer for 10 minutes. After 10 minutes, 2M NaOH (8.0 g NaOH pellets dissolved in 100 mL deionized water) was added dropwise until pH 12 and continue stirring for 2 hours. The pH of solution was tested using universal pH paper. The precipitate obtained was filtered using suction filtration, washed repeatedly with deionized water and absolute ethanol and finally dried in an oven overnight at 60° C.

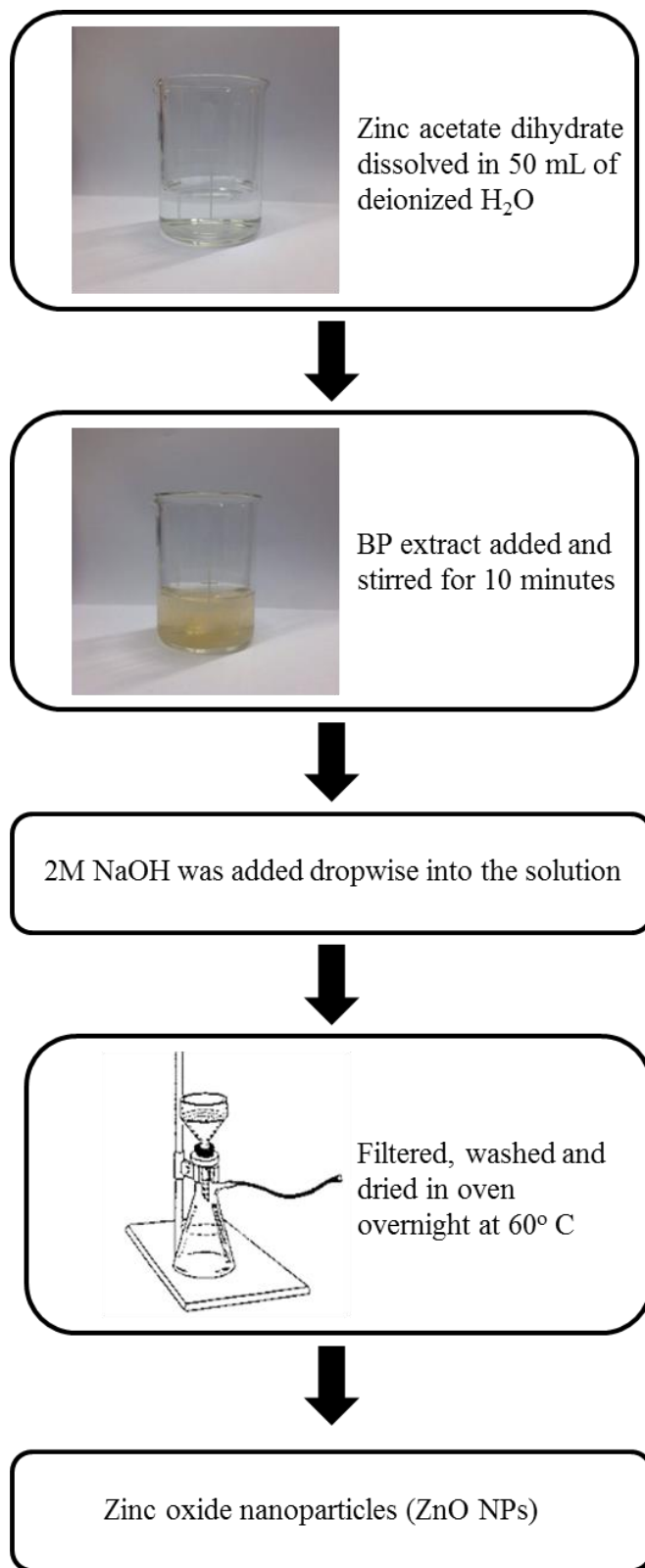


Figure 3.2: Process flowcharts for the preparation of ZnO NPs using BP extract

3.4 Characterization of Synthesized Zinc Oxide Nanoparticles

The synthesized ZnO NPs was characterized using Fourier Transform Infrared Spectroscopy (FTIR), Ultraviolet-Visible (UV-Vis) Spectroscopy, X-ray Diffraction (XRD), Scanning Electron Microscope (SEM), Energy Dispersive X-Ray Spectroscopy (EDX) and Particle Size Analyzer (PSA).

The identification of ZnO NPs crystalline characteristics and its crystalline size were characterized by XRD using Shimadzu XRD 6000 Diffractometer with Cu K α radiation (Voltage = 40 kV, Current = 30 mA, $\lambda = 1.5406\text{\AA}$, scan rate of 2.0°min^{-1} and scan range of 2θ from $10 - 80^\circ$). From the XRD data obtained, the crystalline size of synthesized ZnO NPs was obtained from the Debye-Scherrer's Equation as shown below:-

$$D = \frac{k\lambda}{\beta\cos\theta} \quad (3.1)$$

where,

k = Scherrer constant (usually 0.9)

λ = Wavelength of X-Ray source, Cu K α radiation (1.5406\AA)

β = Full width at half-maximum (FWHM) of the diffraction peak in radian

θ = Bragg's diffraction angle

β obtained from the XRD data was converted to radian unit using the equation shown below:-

$$\beta = \frac{\text{FWHM in } 2\theta \times \pi}{180^\circ} \quad (3.2)$$



Figure 3.3: Shimadzu XRD 6000

FTIR spectra of *Cavendish* BP and the synthesized ZnO NPs were recorded and compared using Perkin Elmer Spectrum RX1 FTIR Spectrometer using KBr pellet method scanning from 4000 cm^{-1} to 400 cm^{-1} . BP was dried in the oven at 60°C , grinded and sieved through a $125 \mu\text{m}$ pore size siever before subjected to FTIR analysis.



Figure 3.4: Perkin Elmer RX 1 FTIR Spectrometer

Optical properties of ZnO NPs were evaluated in the UV-Vis spectrum using Perkin Elmer Lambda 35 UV-Visible Spectrophotometer scanning from 800 nm to 200 nm using deionized water as blank. Sample solution was prepared by dispersing 1 mg of synthesized ZnO NPs in 10 mL of deionized water on a magnetic stirring hotplate with magnetic stirrer.



Figure 3.5: Perkin Elmer Lambda 35 UV-Visible Spectrophotometer

The surface morphology, particle size and elemental analysis of synthesized ZnO NPs were studied using Scanning Electron Microscope (JEOL JSM-6701F) with Oxford Instruments X-Max Energy Dispersive X-ray Diffractometer.



Figure 3.6: JEOL JSM-6701F SEM-EDX

The average particles size of the synthesized ZnO NPs was also determined using Malvern Particle Size Mastersizer 2000.



Figure 3.7: Malvern Particle Size Mastersizer 2000

3.5 Photocatalytic Activity of Synthesized Zinc Oxide Nanoparticles

3.5.1 Preparation of Dye Aqueous Solutions

10 ppm of CR and MG dye aqueous solutions were prepared by dissolving 5 mg of CR and MG powder in a 500 mL volumetric flask containing deionized water. The resulting mixture was magnetically stirred on a magnetic stirring hotplate for 20 minutes to ensure homogeneous dye solutions.

3.5.2 Photocatalytic Dye Degradation

50 mg of photocatalyst, synthesized ZnO NPs was added into a 100 mL beaker containing 50 mL pre-prepared 10 ppm dye aqueous solutions. A total of eight beakers were prepared with the same weight of photocatalyst and volume of dye aqueous solutions. Prior to natural sunlight irradiation, each beaker was magnetically stirred for 30 minutes in dark on magnetic stirring hotplate to achieve the adsorption and desorption equilibrium between photocatalyst with dye molecules. A control was also prepared without the addition of photocatalyst. Then, these beakers were subjected to UV irradiation under natural sunlight within time with strongest light intensity at 12 pm to 3 pm. The light intensity was maintained in the range of 10-12 mW/cm² through measurement using UVA/B

Light Meter 850009. At certain time interval, dye solution with photocatalyst in the beaker was centrifuged using Centrifuge 5430 at 7830 rpm for 5 minutes. The supernatant layers were carefully taken and used to evaluate the photocatalytic activity of ZnO NPs by measuring the absorbance in different wavelength (spectrum) of the supernatant layers collected in different time using Thermo Fischer Scientific Genesys 10S series UV-Visible Spectrophotometer. The number of beakers together with their times to be collected for CR and MG dye solutions were shown in the table below:-

Table 3.1: Time intervals for beakers to be collected during degradation process

No. of Beakers	Time (minutes)	
	CR Dye Aqueous Solution	MG Dye Aqueous Solution
1	Control	Control
2	5	10
3	10	20
4	20	30
5	30	60
6	40	90
7	50	150
8	60	210

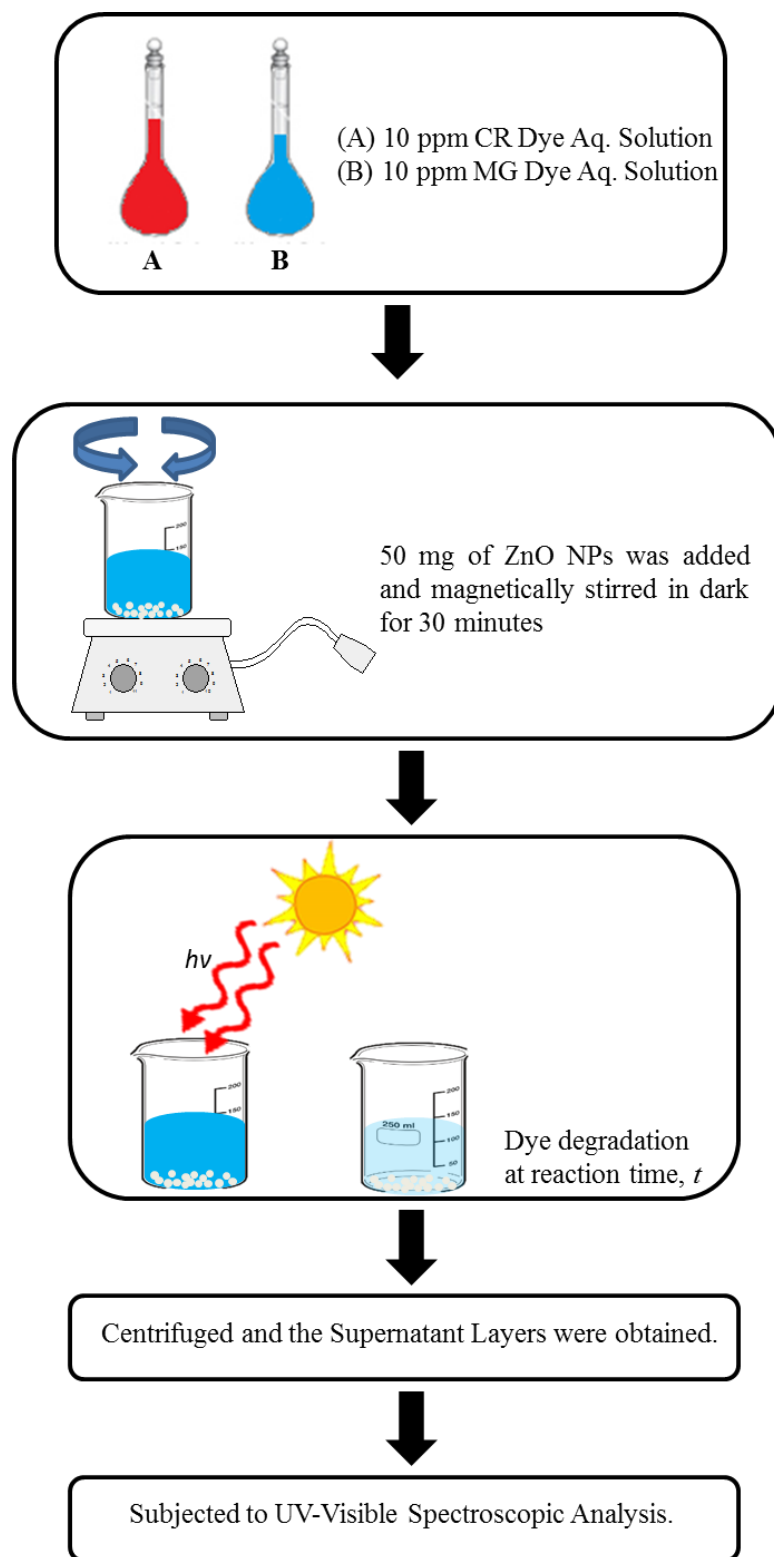


Figure 3.8: Process flowchart of photocatalytic dye degradation under solar irradiation

3.5.3 Determination of Percentage of Degradation

By using the absorbance obtained from the λ_{\max} in visible region of the dye solutions, CR and MG dye solutions are 498 nm and 615 nm respectively, the percentage of dye degradation was estimated using the formula below:-

$$\text{Percentage of Dye Degradation} = \frac{A_0 - A_i}{A_0} \times 100\% \quad (3.3)$$

where,

A_0 = Initial absorbance of dye solutions

A_i = Absorbance of dye solutions at a given contact time

3.5.4 Identification of Degradation Products

The intermediate degradation products formed in the photodegradation process of MG dye aqueous solutions were evaluated using Agilent 6520 Accurate-Mass Hybrid Quadrupole TOF (Q-TOF) Liquid Chromatography-Mass Spectrometry (LC-MS). From the evaluated intermediate products, a tentative degradation pathway of MG was proposed.

CHAPTER 4

RESULTS AND DISCUSSION

4.1 Green Synthesis of Zinc Oxide Nanoparticles

Greyish-white ZnO NPs shown in Figure 4.1 was synthesized using co-precipitation method with the aid of *Cavendish* BP extract. This approach was considered green as it involved the uses of agricultural waste to replace toxic chemical such as surfactants or polymers (to control the growth of particles), universal green solvent, water (H₂O) instead of volatile organic solvent (VOC) and low energy consumption (reaction proceeded in room temperature) that fulfilled the principles of green chemistry.

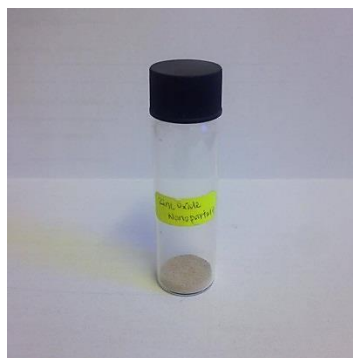


Figure 4.1: Photograph of ZnO NPs synthesized using *Cavendish* BP extract

The synthesis of ZnO NPs involved a redox process. BP extract was first added into salt of zinc acetate dihydrate aqueous solution that reduced Zn(II) to Zn(0) and maintains the size of particles formed in nano scale by capping them from come into contact with each other. A cloudy solution was formed indicates the occurrence of reduction reaction. Sodium hydroxide (NaOH) was added as an accelerant to enhance the rate of reduction and nucleation process by direct precipitation of Zn²⁺ to Zn(OH)₂ in alkaline condition, pH 12 followed by loss of water to form ZnO NPs (Balavandy et al., 2015; Nishimura et al., 2011). The related chemical reactions are shown in the equation below:-



Synthesized ZnO NPs using *Cavendish* BP extract contains impurities on the particle surface. Higher purity was obtained through washing with water followed by ethanol several times during vacuum suction filtration to remove the water soluble and also water insoluble impurities present on the surface of synthesized nanoparticles.

4.2 Characterization of Synthesized Zinc Oxide Nanoparticles

The synthesized greyish-white ZnO NPs was characterized accordingly using total of six techniques which are XRD, EDX, FTIR, UV-Vis Spectroscopy, SEM and PSA.

4.2.1 X-ray Diffraction (XRD)

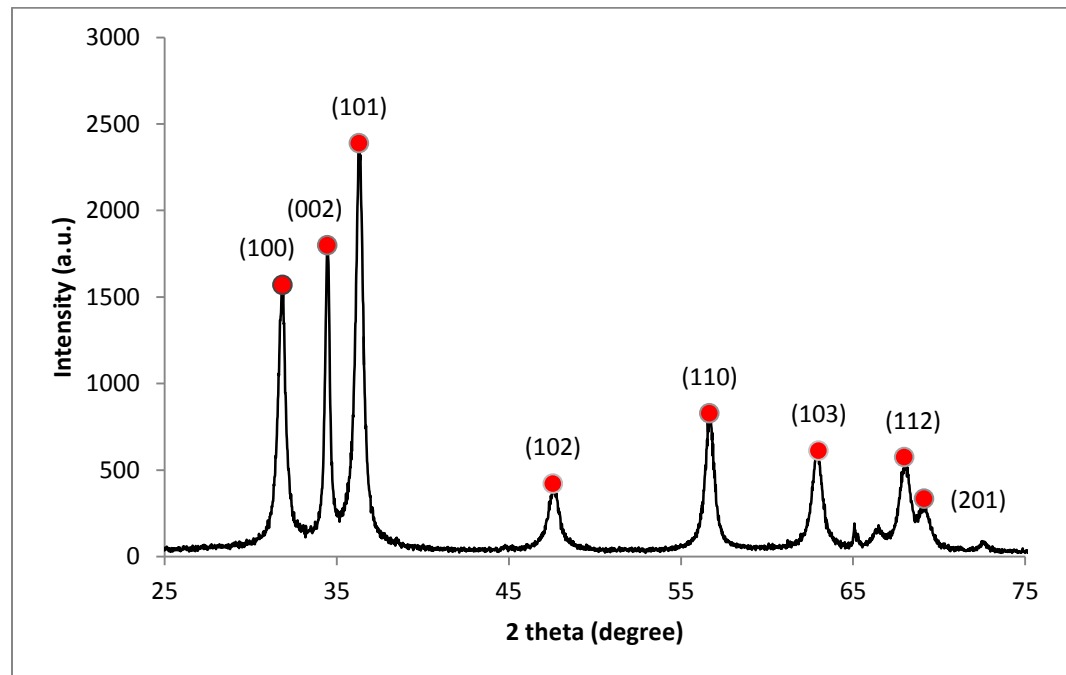


Figure 4.2: XRD Diffractogram of Synthesized ZnO NPs

The observed diffraction peaks in the XRD diffractogram shown in Figure 4.2 at 31.78° (100), 34.43° (002), 36.28° (101), 47.57° (102), 56.62° (110), 62.86° (103), 67.97° (112) and 69.12° (201) which are greatly showed the hexagonal wurtzite structure of ZnO NPs phase by comparing and matched with the standard card of JCPDS Card No. 36-1451 (Zincite) shown in Appendix C. Similar results were also reported by Talam et al., (2012), where the diffraction peaks were located at 31.84° , 34.52° , 36.33° , 47.63° , 56.71° , 62.96° , 68.13° and 69.18° . These diffraction peaks were also observed to be broadening due to the small sizes of particles in nano-scale with moderate crystallinity of 36.58%. Besides, some minor peaks present other than the main peaks between 60° to 80° in the XRD diffractogram reflect to the impurities present on synthesized ZnO NPs. The average crystalline size was also calculated using Debye-Scherrer equation and the calculations were shown in Appendix A. The average crystalline size obtained for the synthesized ZnO NPs is found to be 19.22 nm based on the FWHM of most intense diffraction peak at 36.28° .

4.2.2 Energy Dispersive X-ray Spectroscopy (EDX)

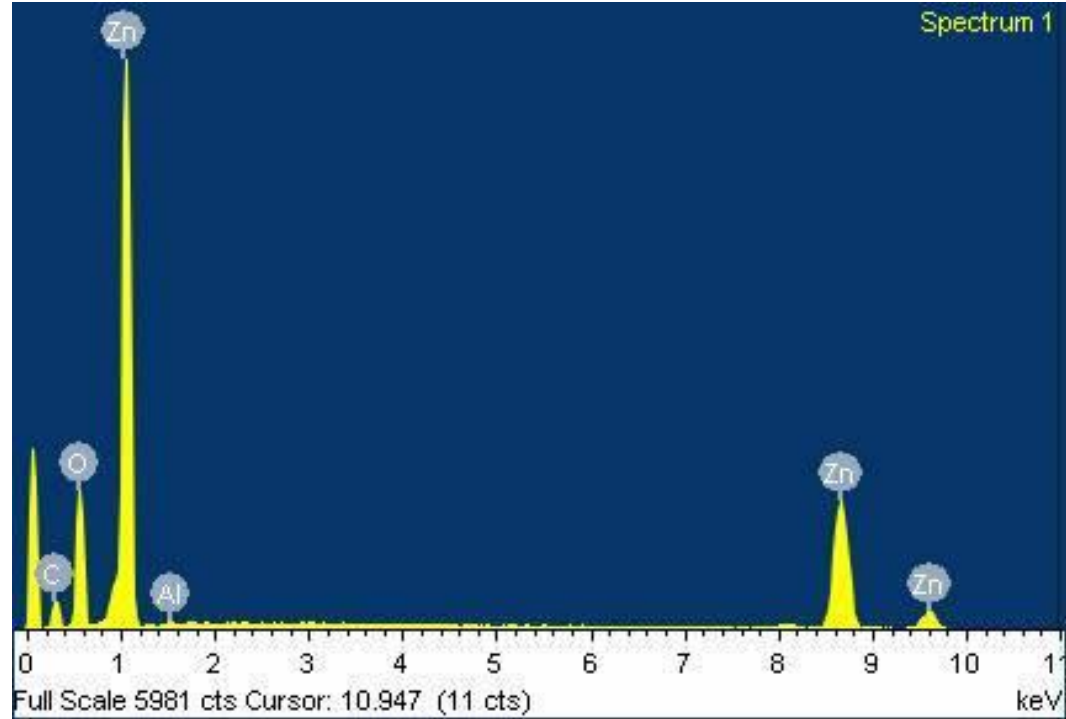


Figure 4.3: EDX spectrum of synthesized ZnO NPs

Table 4.1: EDX analysis processing data

Elements	Weight %	Atomic %
C	17.07	36.13
O	26.19	41.61
Al	0.37	0.35
Zn	56.37	21.92
Total	100.00	100.00

Elemental analysis was done by using EDX spectroscopy and the results are summarized in Figure 4.6 and Table 4.1. There are total of four elements present in the synthesized ZnO NPs which are carbon, oxygen, aluminum and zinc. Carbon occupied unusually high weight %, 17.07 in the ZnO NPs. These carbons are suspected to be come from those organic substituents in the BP extract that served as capping agent remain on the nanoparticles during synthesis. Trace amount of aluminum is also found in the ZnO NPs with weight % of 0.37 which might be contributed by the trace aluminum impurity contained chemicals used during synthesis.

4.2.3 Fourier Transform Infrared Spectroscopy (FTIR)

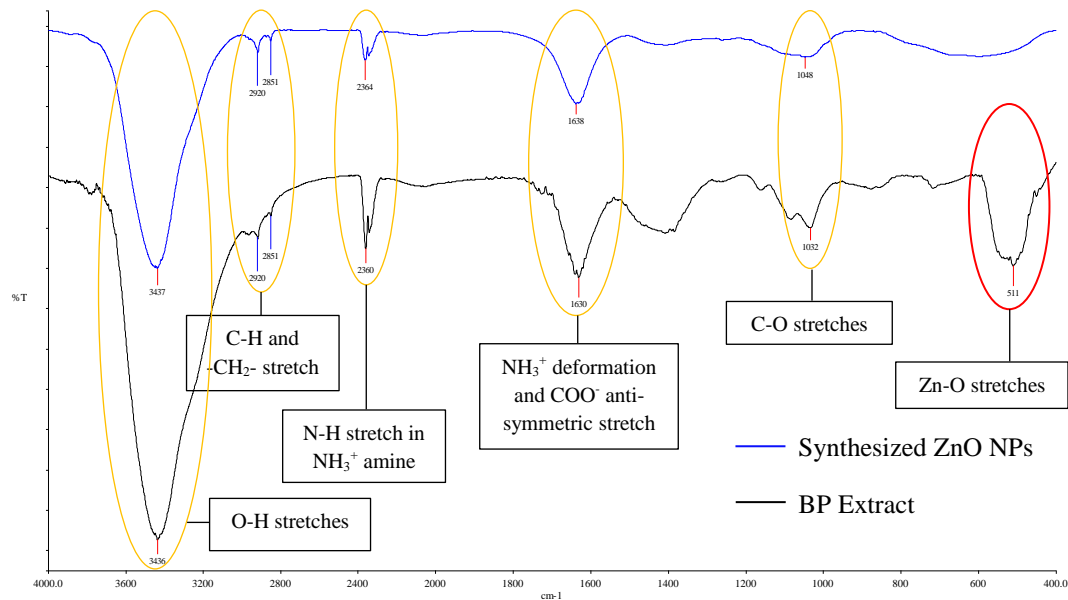


Figure 4.4: FTIR spectra of synthesized ZnO NPs with BP extract

FTIR spectra comparison between synthesized ZnO NPs using BP extract and the BP extract alone is shown in Figure 4.4. Bands shown in between 3500 cm^{-1} to 3200 cm^{-1} belongs to O-H stretches from alcohol, phenol or maybe some water residues remain on the nanoparticles, 2990 cm^{-1} to 2850 cm^{-1} correspond to the symmetric and asymmetric stretching vibrations of C-H in $-\text{CH}_3$ and $-\text{CH}_2-$ of aliphatic chain, 2750 cm^{-1} to 2350 cm^{-1} belongs to the N-H stretching vibrational mode in $-\text{NH}_3^+$ amine, 1580 cm^{-1} to 1640 cm^{-1} are NH_3^+ deformation of NH_3^+ in amino acids or carboxylic acid salt (COO^-) anti-symmetric stretches and 1065 cm^{-1} to 1015 cm^{-1} is the C-O vibrational stretching from an alcohol (C-OH). These

vibrational bands are mostly found in the structures of dopamine and L-DOPA, abundant catecholamine in BP extract as well as others compounds such as cellulose, pectin and hemicellulose. According to Kokila et al., (2015), the shift of bands to lower frequency indicates the participation of these compounds in the synthesis of ZnO NPs. For example, 3437 cm^{-1} shifted to 3436 cm^{-1} , 2364 cm^{-1} to 2360 cm^{-1} , 1638 cm^{-1} to 1630 cm^{-1} and 1048 cm^{-1} to 1032 cm^{-1} . Besides, there is a significant band appeared at 511 cm^{-1} which is owned by Zn-O vibrational stretching that further confirmed the formation of ZnO NPs.

4.2.4 Ultraviolet-Visible Spectroscopy (UV-Vis Spectroscopy)

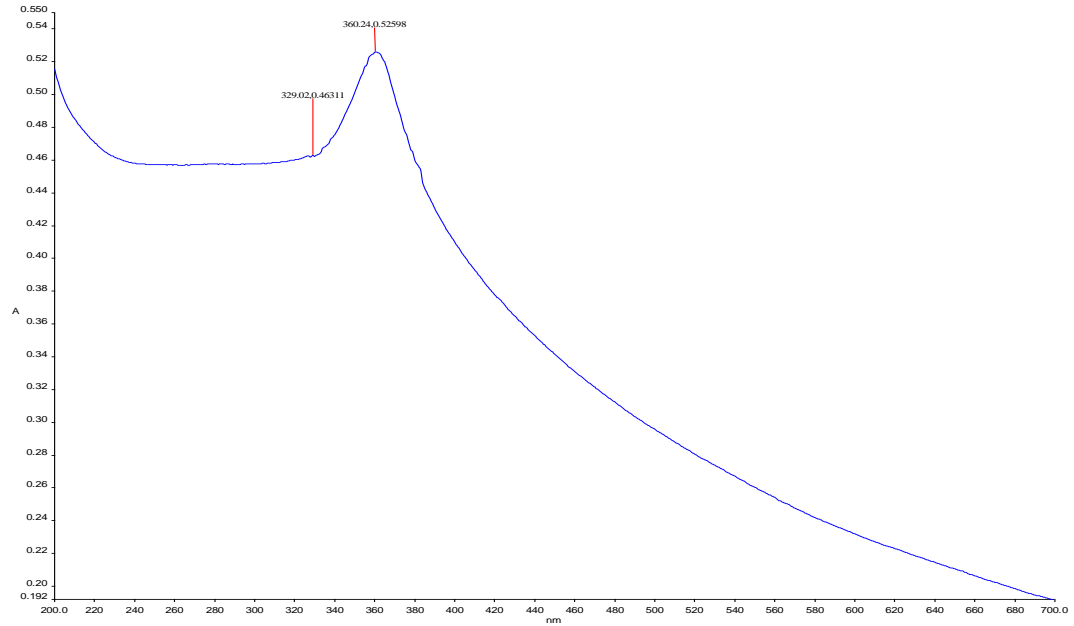


Figure 4.5: UV-Visible spectrum of synthesized ZnO NPs

An intense absorption peak observed in UV-Vis spectrum shown in Figure 4.4 under Ultraviolet (UV) region (200 nm to 400 nm) at 360 nm corresponds to the optical absorption of the synthesized ZnO NPs. The absorption at this wavelength can be related to the band gap energy (E_{bg}) between valence band (VB) and conduction band (CB) of the synthesized semiconductor, ZnO NPs using equation 4.4 where bound electron from VB of semiconductor tends to be excited to CB by absorbing energy from the UV light.

$$E_{bg} = \frac{hc}{\lambda} \quad (4.4)$$

where,

h = Planck's constant ($6.63 \times 10^{-34} \text{ m}^2 \text{ kg s}^{-1}$)

c = Speed of light ($3.00 \times 10^8 \text{ ms}^{-1}$)

λ = Absorption wavelength in UV region (360 nm)

The E_{bg} value calculated from the equation above shown in Appendix G is 3.45 in the unit of eV which is almost the same but slightly higher than theoretical band gap energy value for un-doped ZnO NPs reported by Shamsuzzaman et al., (2014), 3.31 eV, Khan et al., (2013), 3.28 eV as well as the theoretical value, 3.37 eV .

According to Varughese et al., (2015) reported the optical absorption of bulk ZnO occurred near 375 nm and a blue shift (6 nm) could be observed for smaller size ZnO NPs around 369 nm. The absorption wavelength observed in spectrum in this study shown in Figure 4.4, 360 nm is consistent with Varughese et al., (2015) reported data in such a way that ZnO NPs has a blue shifted (15 nm) absorption wavelength than the bulk phase. Therefore, UV-Visible spectroscopy characterization further confirmed the formation of nano-sized ZnO with optical absorption ability.

4.2.5 Scanning Electron Microscope (SEM)

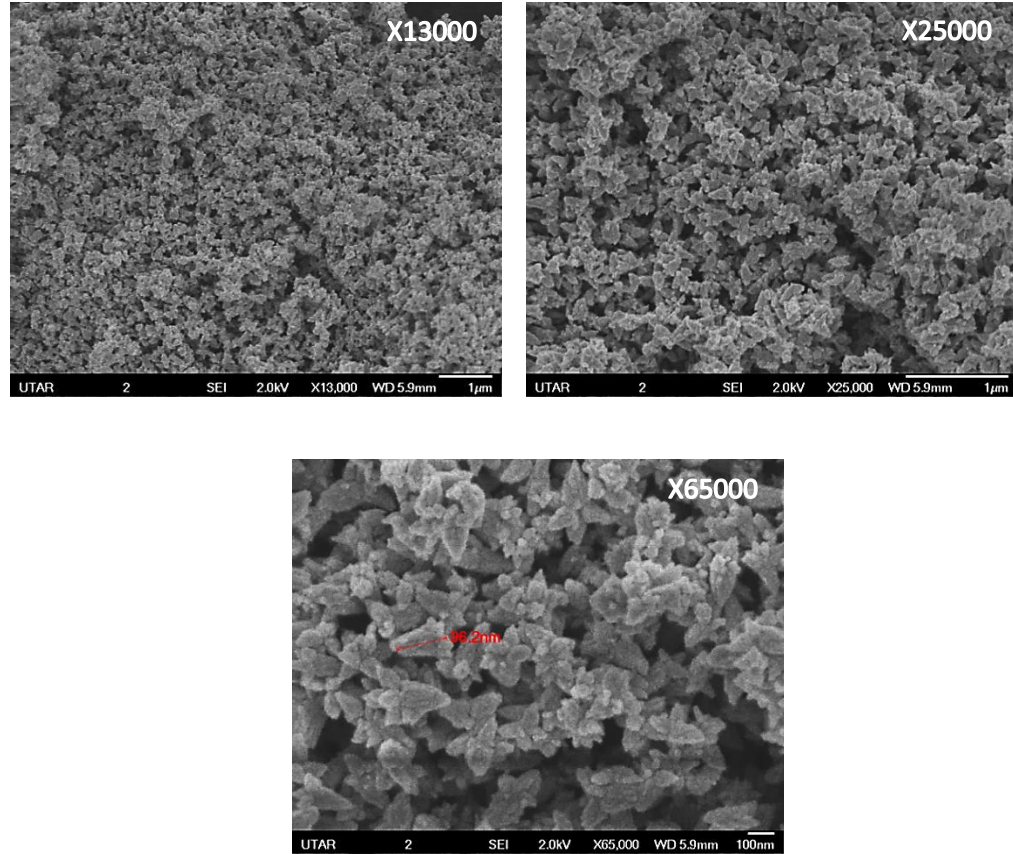
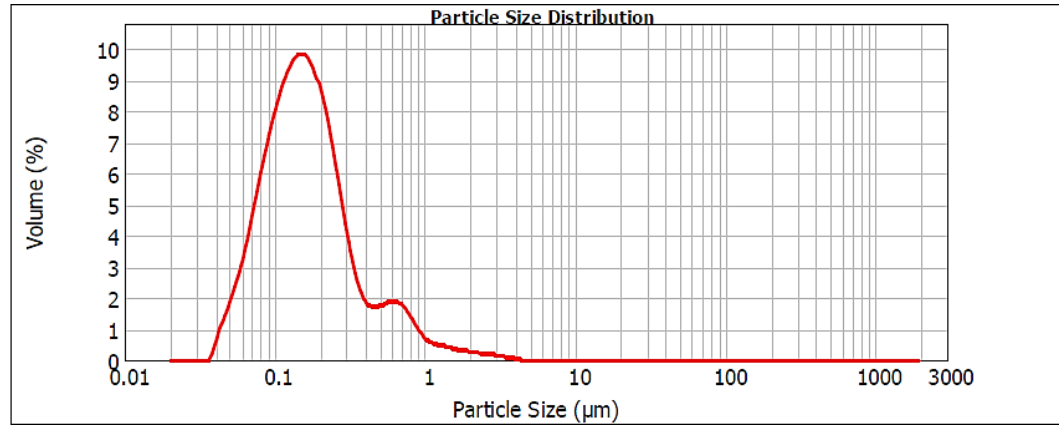


Figure 4.6: SEM images of synthesized ZnO NPs at different magnifications

Surface morphology of synthesized ZnO NPs was studied by observing the images captured under SEM using different magnification shown in Figure 4.5. A huge number of ZnO NPs were aggregated forming a nano-flower like morphology with various irregular shapes of agglomerated particles. A rough idea on the average particle size was also obtained from the given SEM images with a diameter of 96.2 nm.

4.2.6 Particle Size Analyzer (PSA)



Size (µm)	Volume In %	Size (µm)	Volume In %	Size (µm)	Volume In %
0.010	0.00	0.105	7.93	1.096	0.46
0.011	0.00	0.120	8.58	1.259	0.40
0.013	0.00	0.138	8.87	1.445	0.33
0.015	0.00	0.158	8.71	1.660	0.26
0.017	0.00	0.182	8.04	1.905	0.24
0.020	0.00	0.209	6.90	2.188	0.19
0.023	0.00	0.240	5.40	2.512	0.16
0.026	0.00	0.275	3.85	2.884	0.12
0.030	0.00	0.316	2.55	3.311	0.08
0.035	0.06	0.363	1.77	3.802	0.02
0.040	0.91	0.417	1.53	4.365	0.00
0.046	1.56	0.479	1.59	5.012	0.00
0.052	2.36	0.550	1.70	5.754	0.00
0.060	3.36	0.631	1.65	6.607	0.00
0.069	4.64	0.724	1.35	7.586	0.00
0.079	5.88	0.832	0.93	8.710	0.00
0.091	7.01	0.955	0.60	10.000	0.00
0.105		1.096		11.482	

Figure 4.7: Particle size analysis spectrum with processing data

A more specific type of particle size analysis on the synthesized ZnO NPs was done by using PSA. The particle sizes of agglomerated synthesized ZnO NPs were found to be in the range of 138 nm to 158 nm. This range of particle sizes can be considered as consistent with the particle size hypothesized from the SEM Images (96.2 nm) stated in Section 4.2.4. There is also another peak observed in the particle size distribution curve beside the dominant peak (138 nm to 158 nm) within the range of 550 nm to 631 nm that might belongs to the agglomerated ZnO NPs.

4.3 Evaluation of Photocatalytic Activity of Synthesized Zinc Oxide Nanoparticles

Under this section, the photocatalytic activity of the green synthesized ZnO NPs was evaluated through the degradation of a diazo anionic dye (Congo Red) and a cationic dye (Malachite Green) aqueous solution under natural sunlight. Preliminary screening for the occurrence of degradation was done by observing the color fading of dyes aqueous solutions before subjected to optical absorption measurement using UV-Vis spectroscopic analysis. Then, the percentage of degradation was calculated based on the absorbance values obtained to determine the photocatalytic efficiency of the synthesized ZnO NPs.

4.3.1 Degradation of Congo Red Dye In Aqueous Solution Using ZnO NPs under Solar Irradiation

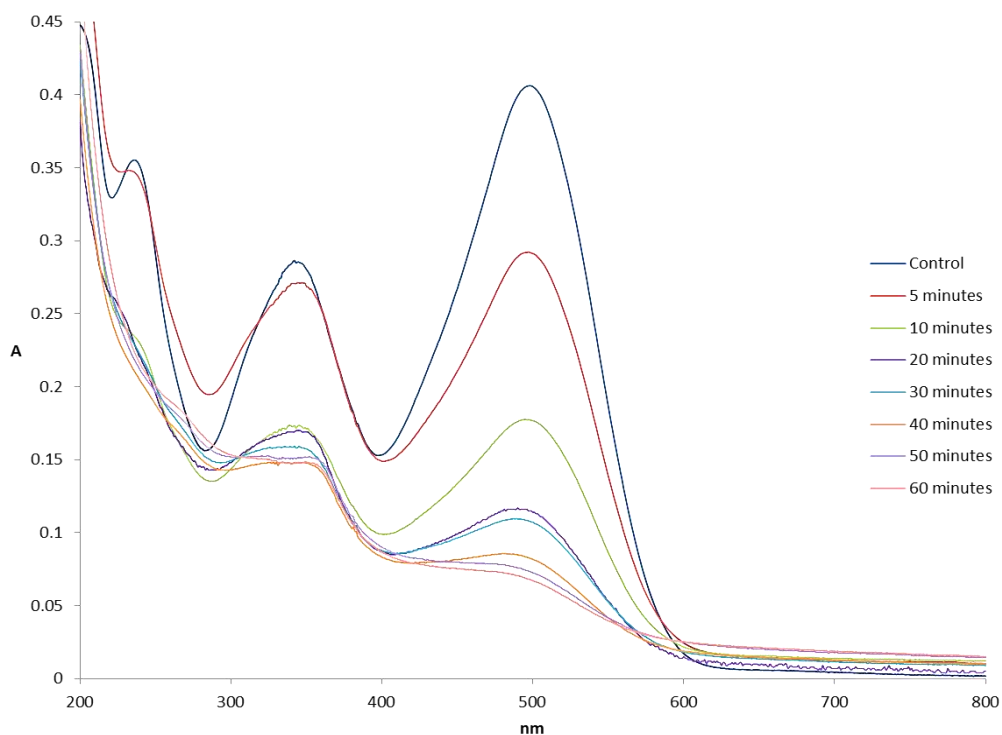


Figure 4.8: UV-Vis spectrum of CR dye degradation as a function of contact time (minutes)

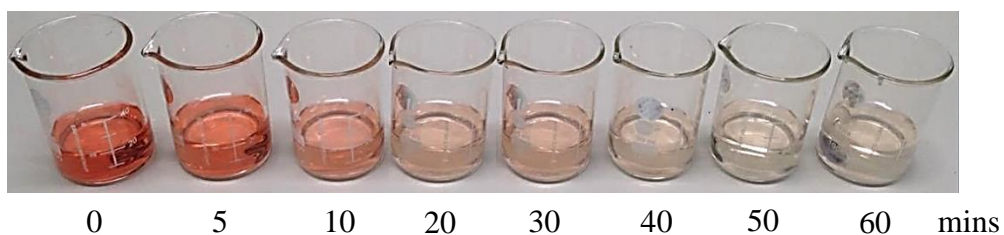


Figure 4.9: Photograph of degraded CR dye aqueous solution in different time interval

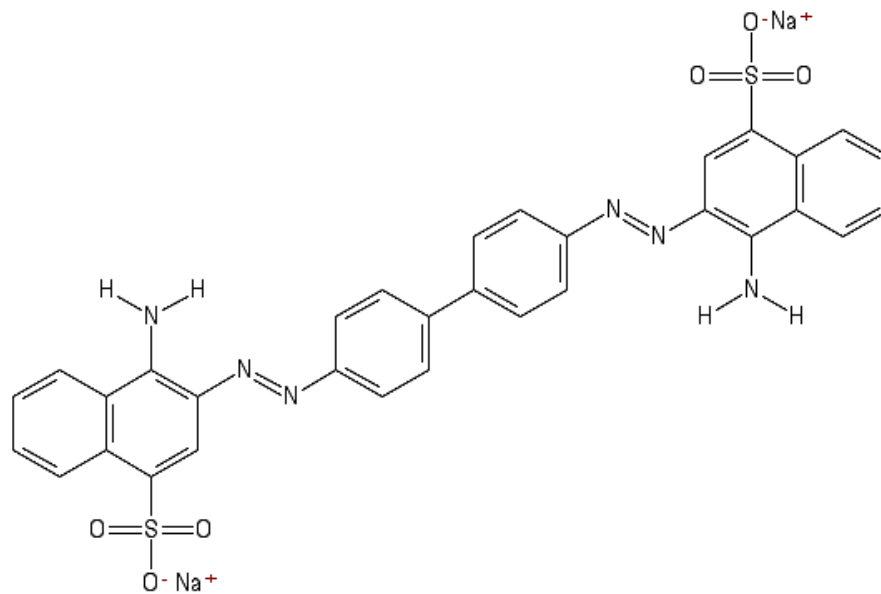


Figure 4.10: Chemical structure of CR dye

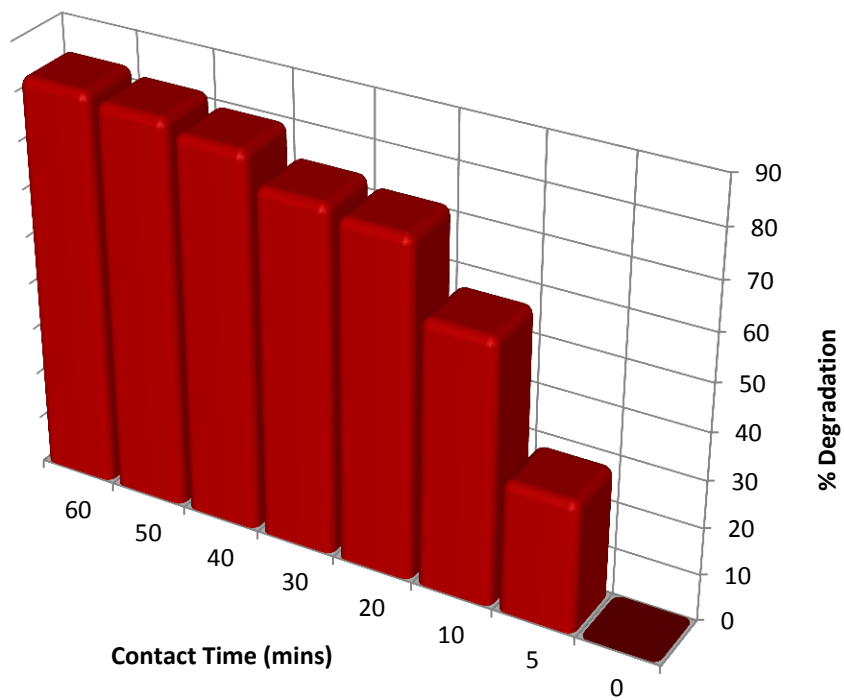


Figure 4.11: Degradation percentage of CR as a function of time

CR is an anionic dye with highly conjugated system between azo bridge, naphthalene and benzene structure shown in Figure 4.10. It appeared to be reddish-orange in color by absorbing energy from the wavelength of blue-green region of visible spectrum. A 10 ppm CR dye aqueous solution was used as a control (0 minutes) for photodegradation with an absorbance value of 0.4063 at $\lambda_{\max} = 498$ nm. Besides, two minor absorption peaks occurred in the UV region at 232 nm and 345 nm belong to the benzene and naphthalene rings chromophores present in the CR molecular structure.

The UV-Vis spectrum shown in Figure 4.8 above reflected the photodegradation of a 10 ppm CR dye aqueous solution using synthesized ZnO NPs in 60 minutes contact time. According to the photograph shown in Figure 4.9, the color of the CR dye aqueous solutions were faded from reddish-orange to orange and turns into pale orange. It is also clearly stated that the absorption peaks at 498 nm were gradually decreasing from the absorbance of 0.4063 at 0 minute to 0.0680 at 60 minutes. The λ_{\max} at 498 nm was disappeared starting from 50 minutes onwards due to the destruction of chromophoric azo (-N=N-) groups from CR molecules accompanied by the decreases in absorbance for 232 nm and 345 nm absorption peaks. There is no new absorption peak was formed in either one region during the degradation process. The percentage degradation of CR dye aqueous solution in 60 minutes contact time was shown in the Figure 4.11 (bar graph) above where the overall percentage of degradation was found to be 83.26%.

4.3.2 Degradation of Malachite Green Dye In Aqueous Solution Using ZnO NPs under Solar Irradiation

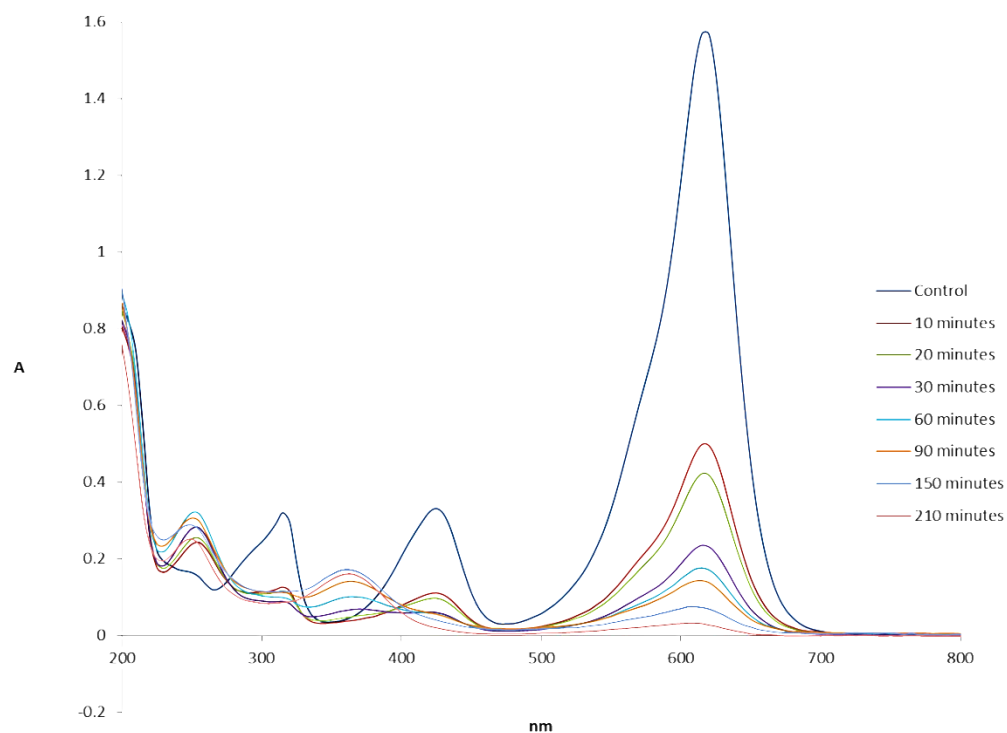


Figure 4.12: UV-Vis spectrum of MG dye degradation as a function of contact time (minutes)

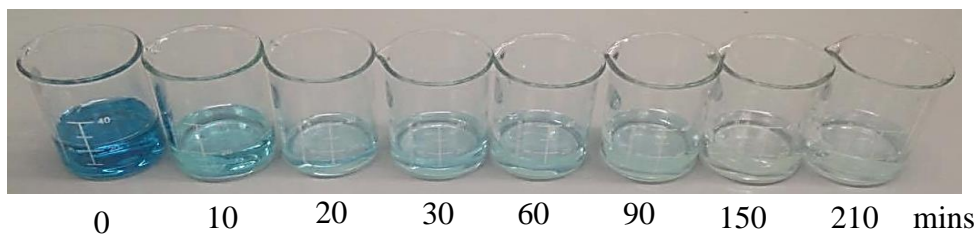


Figure 4.13: Photograph of degraded MG dye aqueous solution in different time intervals

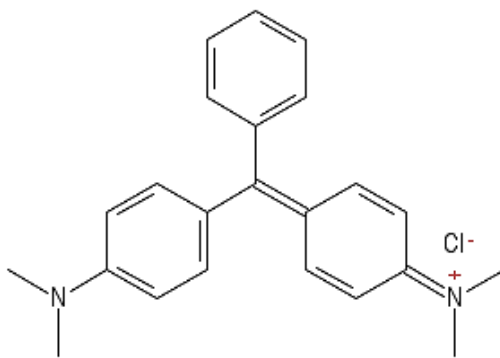


Figure 4.14: Chemical structure of MG dye

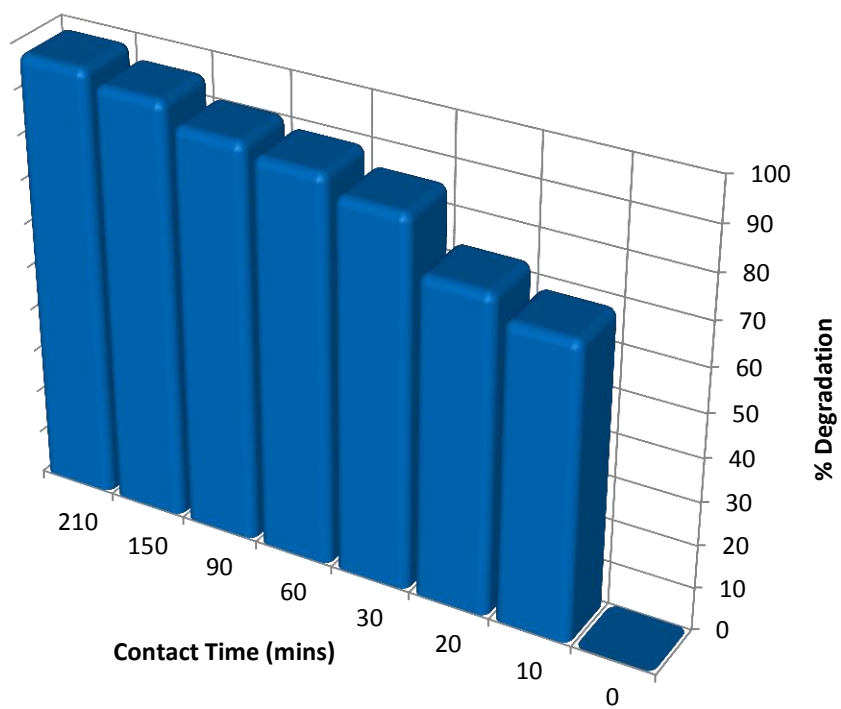


Figure 4.15: Degradation percentage of MG as a function of time

MG is a cationic dye with highly conjugated system in the structure of MG shown in Figure 4.12 that gives rise to its physical appearance of blue-green color in nature by absorbing energy from the wavelength of red region of visible spectrum. A 10 ppm concentration of MG dye aqueous solution was used as the control (0 minute) for the photodegradation with an absorbance value of 1.569 at $\lambda_{\text{max}} = 615$ nm. Besides, two minor absorption peaks appeared at 315 nm and 425 nm respectively correspond to the chromophoric absorption.

According to the photograph in Figure 4.13, the MG dye aqueous solution was first appeared to be blue in color and slowly faded to light blue, sky blue and lastly almost colorless after a 210 minutes contact time. These observations were consistent with the gradually decreasing trends of the major and minor absorption peaks at 315 nm, 425 nm and 615 nm due to the destruction of chromophore groups in the MG structure. However, two new absorption peaks were identified at 250 nm and 360 nm where their absorbance was increasingly formed from 30 minutes contact time until the end of photodegradation process. Both of the peaks could be due to the formation of some intermediate photodegradation products that contain new chromophore groups which is not found in the original MG structure. The percentage degradation of MG dye aqueous solution in 210 minutes contact time was shown in the bar graph below where the overall percentage of degradation was found to be 98.02%.

4.3.3 Adsorption-Desorption and Photodegradation of Dye Aqueous Solution

Photocatalytic degradation involved two processes which are adsorption-desorption and photodegradation. In the first 30 minutes, the percentage degradation of CR and MG dye aqueous solutions were increased drastically to 73.47% and 85.02% respectively and gradually increased after 30 minutes. This is mainly due to the adsorption process of the dye molecules onto the surface of ZnO NPs. Similar phenomenon was reported by Ljubas et al., (2015) that the CR dye solution gives 60% reduction of absorbance for the first 5 minutes under ultrasonication stirring due to the adsorption of CR dye molecules onto the surface of TiO₂ nanoparticles.

There are two types of adsorption which are physisorption and chemisorption. Physisorption involved the formation of weak Vander Waals Forces between the photocatalyst and dye molecules whereas chemisorption can be occur through hydrogen bonding or electrostatic attraction. According to Elaziouti et al., (2011), the isoelectric point of ZnO NPs is $\text{pH}_{\text{zpc}} = 9.0$ and the surface charge of ZnO NPs is strongly depends on the pH of the solution according to the equations shown below:-

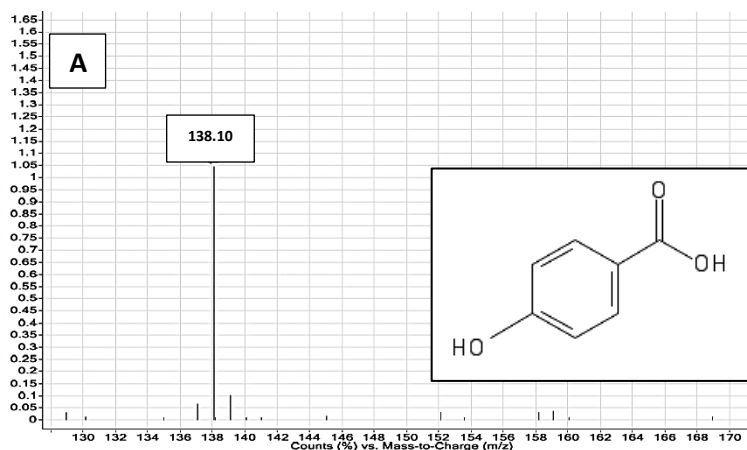


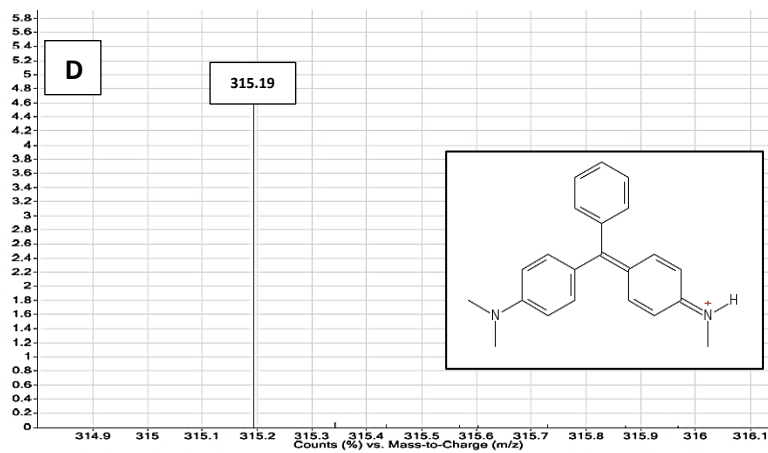
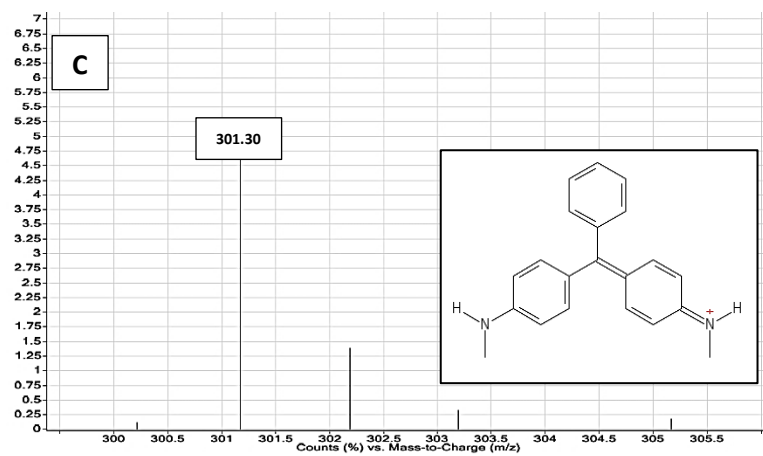
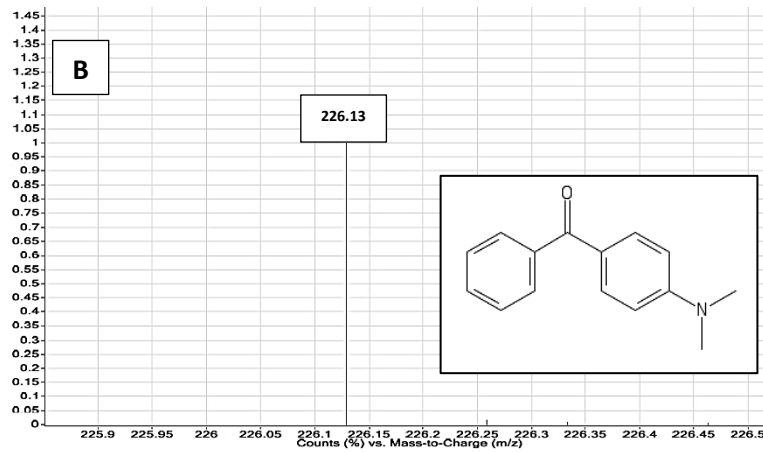
In this study, neutral ($\text{pH} \approx 7$) pH dye aqueous solutions were used in order to compromise the concentration of OH^- and dye molecules on the surface of ZnO NPs. The surface charge of ZnO NPs tends to be positively charge ($\text{pH} 7 < \text{pH}_{\text{zpc}}$) that can be interact with anionic dye molecules as well as OH^- via electrostatic attraction that favor the photodegradation process. Besides, anionic and cationic dye molecules can also bind to the surface of ZnO NPs via hydrogen bonding through the sulphonate or amine groups for CR dye molecules and amine groups for MG dye molecules (Bagheri et al., 2014).

As the contact time goes on, adsorption sites on the surface of ZnO NPs were increasingly loaded. Adsorption rate will be much slower as it has reached the saturation point where most of the adsorption sites have been filled up. Once the dye molecule reached the surface of photocatalyst, degradation was initiated by the powerful oxidant (HO^\cdot) produced on the surface of ZnO NPs and leaves the degradation end-product, CO_2 followed by adsorption of another dye molecule. These adsorption and degradation processes are time consuming and therefore, the absorbance at 498 nm and 615 nm declined in a slower rate (% degradation from 73.47% to 83.26% for CR and 85.02% to 98.02% for MG dye aqueous solutions) after 30 minutes contact time.

4.3.4 Identification of Degradation Products for MG Dye Aqueous Solution by Liquid Chromatography-Mass Spectrometry (LC-MS)

Photocatalytic degradation of MG dye aqueous solution using ZnO NPs involved the oxidation of dye molecules by a very powerful oxidizing agent, hydroxyl radicals (HO^\cdot) via free radical mechanism. Therefore, a series of intermediate degradation products were formed and analyzed using LC/MS. There are total of 7 compounds have been identified as intermediate products as well as the original MG molecules according to their mass-to-charge (m/z) ratio in the MS spectrum shown in Figure 4.16 below.





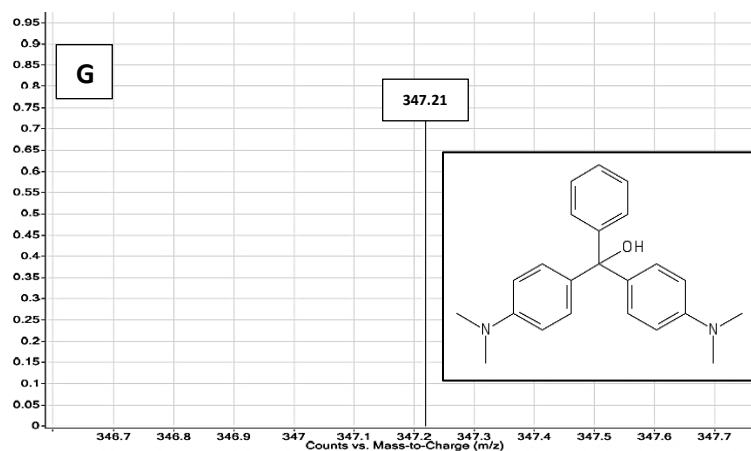
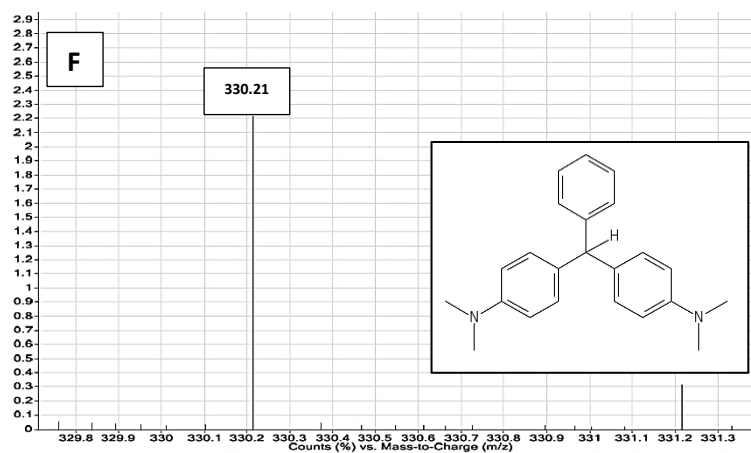
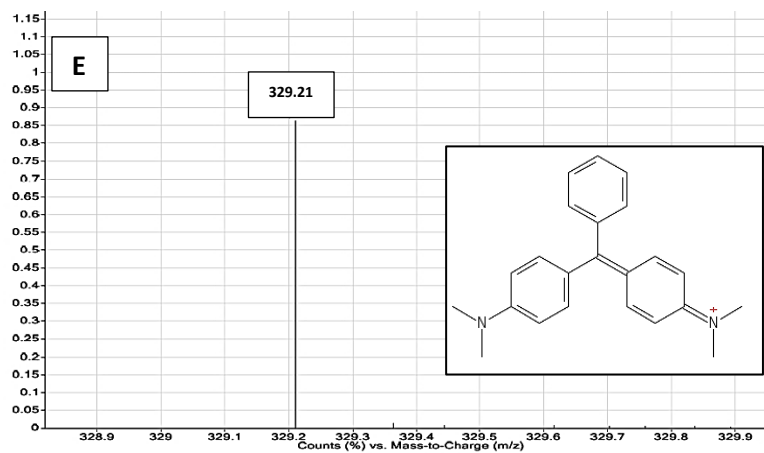


Figure 4.16: Mass spectra of (A) 4-hydroxybenzoic acid, (B) 4-(dimethylamino)-benzophenone, (C) didesmethyl MG, (D) desmethyl MG, (E) MG, (F) Leuco MG and (G) MG leucocarbiniol

There are still quite a number of unknown intermediate products are yet to identify during the photodegradation process but in this study, only these products were identifiable. Based on the intermediate products identified, a tentative degradation pathway of MG dye aqueous solution was proposed according to the study reported by Diao et al., 2013 and Chen et al., 2007 shown in Figure 4.17 below.

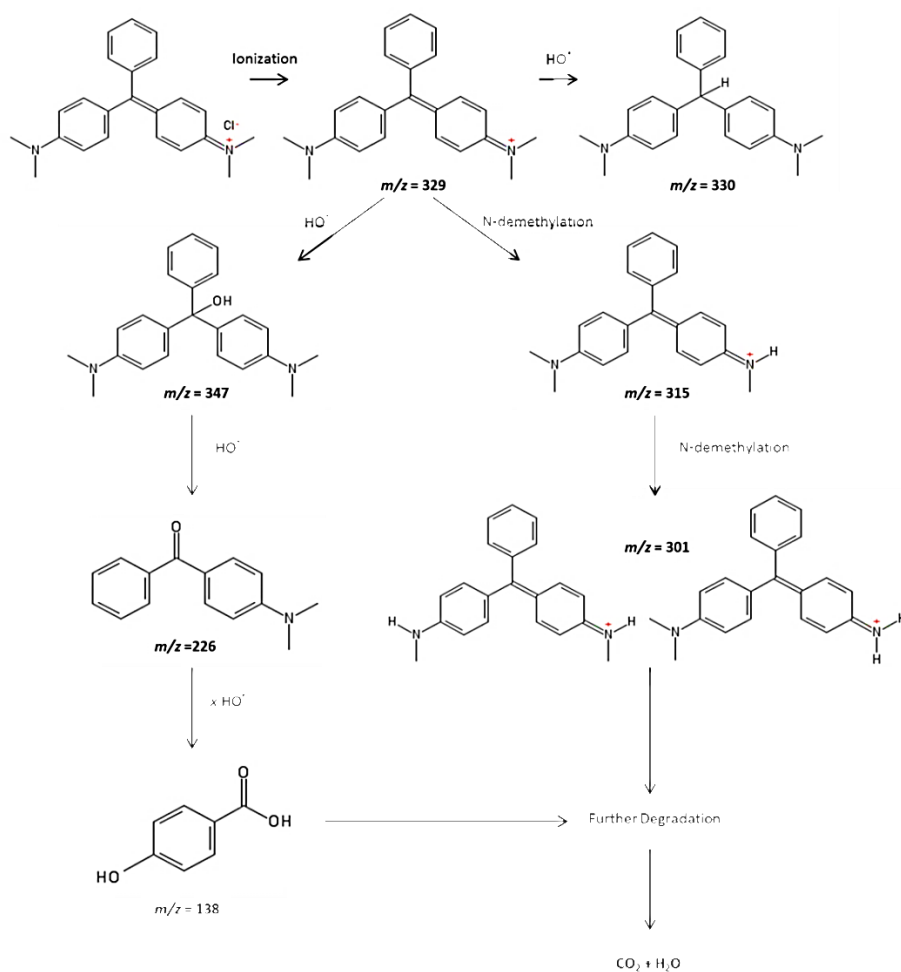


Figure 4.17: Tentative degradation pathway of MG dye in aqueous solution using ZnO NPs

Degradation was initiated by ionization of MG forming a positively charged on the nitrogen atom. Two possible degradation pathways occurred on MG dye molecules either through N-demethylation forming desmethyl MG ($m/z = 315$) or undergoing hydroxylation that attack by hydroxyl radical forming MG leucocarbinol ($m/z = 347$).

- N-demethylation pathway: desmethyl MG tends to undergo N-demethylation once again forming didesmethyl MG ($m/z = 301$) followed by a series of degradation processes end up with the mineralized products, CO_2 and H_2O .
- Hydroxylation pathway: MG leucocarbinol formed was oxidized by HO^\cdot forming 4-(dimethylamino)-benzophenone ($m/z = 226$) followed by a series of oxidation, demethylation and deamination produced 4-hydroxybenzoic acid ($m/z = 138$) then mineralized to CO_2 and H_2O .

CHAPTER 5

CONCLUSION

In this study, ZnO NPs has been successfully synthesized through a green synthetic pathway with the aid of *Cavendish* BP extract as reducing agent as well as stabilizing agent. The synthesized ZnO NPs was characterized using XRD, EDX, FTIR, UV-Vis spectroscopy, SEM and PSA. The particle size of synthesized ZnO NPs in the range between 138 nm to 158 nm observed from the particle size distribution curve and crystalline size 19.22 nm calculated from Debye-Scherrer's Equation according to the highest diffraction peaks in the XRD diffractogram. SEM images revealed the morphology of synthesized ZnO NPs as nano-flowers with various irregular shapes of agglomerated particles.

According to the analysis on photodegradation of CR anionic and MG cationic dye aqueous solutions, the synthesized ZnO NPs shows an excellent photocatalytic activity towards CR and MG dyes as dye solutions have been successfully degraded up to 83.26% in 60 minutes contact time and 98.02% in 210 minutes contact time respectively. Several intermediates degradation products for MG dye have been identified through the LC-MS analysis and based on these identified intermediates, a tentative degradation pathway has been proposed.

However, there are still quite a number of intermediates are un-identifiable. In order to view on the overall degradation pathway of MG dye molecules, further work is required. Couple the data from LC-MS as well as GC-MS could be one of the possible ways to further identify and confirm the presence of some intermediates formed in the photodegradation process. Furthermore, the determination of intermediate degradation products is not done on the photodegradation of CR dye in this study due to time constraint, therefore LC-MS and GC-MS can also be applied to identify, analyze and proposed a possible degradation pathway for CR dye aqueous solution.

REFERENCES

Journal:

- Ahmed, S., Ahmad, M., Swami, B. L. and Ikram, S. (2016). A review on plants extract mediated synthesis of silver nanoparticles for antimicrobial applications: a green expertise. *Journal of Advance Research.*, 7, pp.17-28.
- Ahmed, W. S., Mohamed, M. A., El-Dib, R. A. and Hamed, M. M. (2009). New triterpene saponins from *Duranta repens* Linn. and their cytotoxic activity. *Molecules*, 4, pp.1952-1965.
- Aqil, F., Ahmad, I. and Mehmood, Z. (2006). Antioxidant and free radical scavenging properties of twelve traditionally used Indian medicinal plants. *Turk J Biol*, 30, pp.177-183.
- Bagheri, M., Mahjoub, A. R. and Mehri, B. (2014). Enhanced photocatalytic degradation of congo red by solvothermally synthesized CuInSe₂-ZnO nanocomposites. *RSC Advances*, 4, pp.21757-21764.
- Balavandy, S. K., Shameli, K. and Abidin, Z. Z. (2015). Rapid and green synthesis of silver nanoparticles via sodium alginate media. *International Journal of Electrochemical Science*, 10, pp.486-497.
- Bheemanagouda, N., Patil, N. and Taranath, T. C. (2016). *Limonia acidissima* L. leaf mediated synthesis of zinc oxide nanoparticles: a potent tool against *Mycobacterium tuberculosis*. *International Journal of Mycobacteriology*, 5, pp.197-204.

- Chen, C. C., Lu, C. S., Chung, Y. C. and Jan, J. L. (2007). UV light induced photodegradation of malachite green on TiO₂ nanoparticles. *Journal of Hazardous Materials*, 141, pp.520-528.
- Curri, M. L., Comparelli, R., Cozzoli, P. D., Mascolo, G. and Agostiano, A. (2003). Colloidal oxide nanoparticles for the photocatalytic degradation of organic dye. *Materials Science and Engineering*, 23, pp.285-289.
- Davar, F., Majedi, A. and Mirzaei, A. (2015). Green synthesis of ZnO nanoparticles and its application in the degradation of some dyes. *Journal of the American Ceramic Society*, 98(6), pp.1739-1746.
- Demir, N., Yildiz, O., Alpaslan, M. and Hayaloglu, A. A. (2014). Evaluation of volatiles, phenolic compounds and antioxidant activities of rose hip (*Rosa L.*) fruits in Turkey. *LWT- Food Science and Technology*, 57, pp.126-133.
- Devendran, G. and Balasubramanian, U. (2011). Qualitative phytochemical screening and GC-MS analysis of *Ocimum sanctum* L. leaves. *Asian Journal of Plant Science and Research*, 1(4), pp.44-48.
- Diao, Z. H., Li, M. Y., Zeng, F. Y., Song, L. and Qiu, R. L. (2013). Degradation pathway of malachite green in a novel dual-tank photoelectrochemical catalytic reactor. *Journal of Hazardous Materials*, 260, pp.585-592.
- Dobrucka, R. and Dugaszewska, J. (2016). Biosynthesis and antibacterial activity of ZnO nanoparticles using *Trifolium pratense* flower extract. *Saudi Journal of Biological Sciences*, 23, pp.517-523.
- Elaziouti, Laouedj, N. and Ahmed, B. (2011). ZnO-assisted photocatalytic degradation of congo red and benzopurpurine 4B in aqueous solution. *Journal of Chemical Engineering & Process Technology*, 2(2), pp.1-9.

- Giwa, A., Nkeonye, P. O., Bello, K. A. and Kolawole, K. A. (2012). Photocatalytic decolourization and degradation of C.I. basic blue 41 using TiO₂ nanoparticles. *Journal of Environment Protection*, 3, pp.1063-1069.
- Gnanasangeetha, D. and Thambavani, S. D. (2014). Facile and eco-friendly method for the synthesis of zinc oxide nanoparticles using *Azadirachta* and *Emblica*. *International Journal of Pharmaceutical Sciences And Research*, 5(7), pp.2866-2873.
- Gonzalez-Montelongo, R., Lobo, M. G. and Gonzalez, M. (2010). Antioxidant activity in banana peel extracts: testing extraction conditions and related bioactive compounds. *Food Chemistry*, 119, pp.1030-1039.
- Jafarirad, S., Mehrabi, M., Divband, B. and Kosari-Nasab, M. (2016). Biofabrication of zinc oxide nanoparticles using fruit extract of *Rosa canina* and their potential against bacteria: a mechanistic approach. *Materials Science and Engineering C*, 59, pp.296-302.
- Jagtap, U. B. and Bapat V. A. (2010). *Artocarpus*: A review of its traditional uses, phytochemistry and pharmacology. *Journal of Ethnopharmacology*, 129, pp.142-166.
- Jodko-Piorecka, K. and Litwinienko, G. (2015). Antioxidant activity of dopamine and L-DOPA in lipid micelles and their cooperation with an analogue of α -tocopherol. *Free Radical Biology and Medicine*, 83, pp.1-11.
- Joshi, B., Sah, G. P., Basnet, B. B., Bhatt, M. R., Sharma, D., Subedi, K., Pandey, J. and Malla, R. (2010). Phytochemical extraction and antimicrobial properties of different medicinal plants: *Ocimum sanctum* (tulsi), *Eugenia caryophyllata* (clove), *Achyranthes bidentata* (datiwan) and *Azadirachta indica* (neem). *Journal of Microbiology and Antimicrobials*, 3(1), pp.1-7.

- Kavitha, K. S., Baker, S., Rakshith, D., Kavitha, H.U., Yashwantha, R. H. C., Harini, B. P. and Satish, S. (2013). Plants as green source towards synthesis of nanoparticles. *International Research Journal of Biological Sciences*, 2(6), pp.66-76.
- Khan, W., Khan, Z. A., Saad, A. A., Shervani, S., Saleem, A. and Naqvi, A. H. (2013). Synthesis and characterization of Al doped ZnO nanoparticles. *International Journal of Modern Physics: Conference Series*, 22, pp.630-636.
- Khanal, D. P., Raut, B., Majhi, R. K., Kaini, A., Basnet, R. and Mahat, P. K. (2014). Phytochemical and biological studies on fruits of *Duranta repens* L.. *An International Journal of Advances in Pharmaceutical Sciences*, 5(2), pp.1958-1962.
- Klejduš, B., Vitamvasova-Sterbova, D. and Kuban, V. (2001). Identification of isoflavone conjugates in red clover (*Trifolium pratense*) by liquid chromatography-mass spectrometry after two-dimensional solid-phase extraction. *Analytical Chimica Acta*, 450, pp.81-97.
- Kokila, T., Ramesh, P. S. and Geetha, D. (2015). Biosynthesis of silver nanoparticles from *Cavendish* banana peel extract and its antibacterial and free radical scavenging assay: a novel biological approach. *Applied Nanoscience*, 5, pp.911-920.
- Kolodziejczak-Radzimska, A. and Jesionowski, T. (2014). Zinc oxide-from synthesis to application: a review. *Materials*, 7, pp.2833-2881.
- Krishnamurthy, S. R. and Sarala, P. (2013). Phytochemical studies of *Artocarpus gomezianus* fruits collected from various altitudes of Central Western Ghats. *Indian Journal of Natural Products and Resources*, 4(4), pp.398-411.
- Kumar, R., Singh, V. P., Maurya, D and Pandey, A. K. (2015). Bionanoparticles: a green nanochemical approach. *PharmaTutor*, 3(9), pp.28-35.

- Ljubas, D., Smoljanic, G. and Juretic, H. (2015). Degradation of methyl orange and congo red dyes by using TiO₂ nanoparticles activated by the solar and the solar-like radiation. *Journal of Environment Management*, 161, pp.83-91.
- Lorente, J., Vegara, S., Mart, N., Ibarz, A., Coll, L., Hernandez, J., Valero, M. and Saura, D. (2014). Chemical guide parameters for Spanish lemon (*Citrus limon* (L.) Burm.) juices. *Food Chemistry*, 162, pp.186-191.
- Martel, R., Schmidt, T., Shea, H., Hertel, T. and Avouris, P. (1998). Single- and multi-wall carbon nanotube field-effect transistors. *Applied Physics Letters*, 73(17), pp.2447-2449.
- Nagajyothi, P. C., An, T. N. M., Sreekanth, T. V. M., Lee, J., Lee, D. J. and Lee, K. D. (2013). Green route biosynthesis: characterization and catalytic activity of ZnO nanoparticles. *Materials Letters*, 108, pp.160-163.
- Nishimura, S., Mott, D., Takagaki, A., Maenosono, S. and Ebitani, K. (2011). Role of base in the formation of silver nanoparticles synthesized using sodium acrylate as a dual reducing and encapsulating agent. *Physical Chemistry Chemical Physics*, 13, pp.9335-9343.
- Nogata, Y., Sakamoto, K., Shiratsuchi, H., Ishii, T., Yano, M. and Ohta, H. (2006). Flavonoid composition of fruit tissues of citrus species. *Bioscience, Biotechnology, and Biochemistry*, 70(1), pp.178-192.
- Oudhia, A., Kulkarni, P. and Sharma, S. (2015). Green synthesis of ZnO nanotubes For bioapplications. *International Journal of Advanced Engineering Research and Studies*, pp.280-281.
- Pandavadra, M. and Chanda, S. (2014). Development of quality control parameters for the standardization of *Limonia acidissima* L. leaf and stem. *Asian Pacific Journal of Tropical Medicine*, 7(1), pp.244-248.

- Penner, R. M., Walter, E. C., Zach, M. P., Favier, F., Murray, B. J., Inazu, K. and Hemminger, J. C. (2003). Metal nanowire arrays by electrodeposition. *Chemphyschem*, 4, pp.131-138.
- Poinern, G. E. J., Tripathy, S. K., Sharma, S., Fawcett, D. and Shah, M. (2015). Green synthesis of metallic nanoparticles via biological entities. *Materials*, 8, pp.7278-7308.
- Ramesh, P., Rajendran, A. and Meenakshisundaram, M. (2014). Green synthesis of zinc oxide nanoparticles using flower extract *Cassia auriculata*. *Journal of NanoScience and NanoTechnology*, 2(1), pp.41-45.
- Raut, S., Thorat, P. V., Thakre, R. (2013). Green synthesis of zinc oxide (ZnO) nanoparticles using *Ocimum tenuiflorum* leaves. *International Journal of Science and Research*, 4(5), pp.1225-1228.
- Sabir, S., Arshad, M. and Chaudhari, S. K. (2014). Zinc oxide nanoparticles for revolutionizing agriculture: synthesis and applications. *The Scientific World Journal*, pp.1-8.
- Saravanan, P., Gopalan, R. and Chandrasekaran, V. (2008). Synthesis and characterization of nanomaterials. *Defence Science Journal*, 58(4), pp.504-516.
- Saviranta, N. M. M., Julkunen-Tiitto, R., Oksanen, E. and Karjalainen, R. O. (2010). Leaf phenolic compounds in red clover (*Trifolium pratense* L.) induced by exposure to moderately elevated ozone. *Environmental Pollution*, 158, pp.440-446.
- Senthilkumar, S. R. and Sivakumar, T. (2014). Green tea (*Camellia sinensis*) mediated synthesis of zinc oxide (ZnO) nanoparticles and studies on their antimicrobial activities. *International Journal of Pharmacy and Pharmaceutical Sciences*, 6(6), pp.461-465.

- Shah, R. K., Boruah, F. and Parween, N. (2015). Synthesis and characterization of ZnO nanoparticles using leaf extract of *Camellia sinesis* and evaluation of their antimicrobial efficacy. *International Journal of Current Microbiology and Applied Sciences*, 4(8), pp.444-450.
- Shamsuzzaman, Ali, A., Asif, M., Mashrai, A. and Khanam, H. (2014). Green synthesis of ZnO nanoparticles using *Bacillus subtilis* and their catalytic performance in the one-pot synthesis of steroidal thiophenes. *European Chemical Bulletin*, 3(9), pp.939-945.
- Sharma, P., Khandelwal, S., Singh, T. and Vijayvergia, R. (2012). Phytochemical analysis and antifungal potential of *Duranta erecta* against some phytopatogenic fungi. *International Journal Of Pharmaceutical Sciences and Research*, 3(8), pp.2686-2689.
- Shekhawat, M. S., Ravindran, C. P. and Manokari, M. (2016). Biogenic production of zinc oxide nanoparticles from aqueous extracts of *Duranta erecta* L. *World Scientific News*, 28, pp.30-40.
- Suresh, D., Shobharani, R. M., Nethravathi, P. C., Kumar, M. A. P., Nagabhushana, H. and Sharma, S. C. (2015). *Artocarpus gomezianus* aided green synthesis of ZnO nanoparticles: luminescence, photocatalytic and antioxidant properties. *Spectrochimica Acta Part A: Molecular and Biomolecular Spectroscopy*, 141, pp.128-134.
- Talam, S., Karumuri, S. R. and Gunnam, N. (2012). Synthesis, characterization, and spectroscopic properties of ZnO nanoparticles. *ISRN Nanotechnology*, 2012, pp.1-6.
- Thitilertdecha, N., Teerawutgulrag, A. and Rakariyatham, N. (2008). Antioxidant and antibacterial activities of *Nephelium lappaceum* L. extracts. *Food Science and Technology*, 41, pp.2029-2035.

Varghese, E. and George, M. (2015). Green synthesis of zinc oxide nanoparticles. *International Journal of Advanced Research In Science And Engineering*, 4(1), pp.307-314.

Varughese, G., Jithin, P. W. and Usha, K. T. (2015). Determination of optical band gap energy of wurtzite ZnO: Ce nanocrystallites. *Physical Science International Journal*, 5(2), pp.146-154.

Veerasamy, R., Tiah, Z. X., Gunasagaran, S., Foo, W. X., Fang, C. Y., Jeyakumar, N. and Dhanaraj, S. A. (2010). Biosynthesis of silver nanoparticles using mangosteen leaf extract and evaluation of their antimicrobial activities. *Journal of Saudi Chemical Society*, 15, pp.113-120.

Yuvakkumar, R., Suresh, J., Nathanael, A. J., Sundrarajan, M. and Hong, S. I. (2014). Novel green synthetic strategy to prepare ZnO nanocrystals using rambutan (*Nephelium lappaceum* L.) peel extract and its antibacterial applications. *Materials Science and Engineering*, 41, pp-17-27.

Edited Book:

Ahmad, N., Anwar, F. and Gilani, A. U. (2016). Rose hip (*Rosa canina* L.) oils. In: Preedy, V. R., eds. *Essential Oils in Food Preservation, Flavor and Safety*. Academic Press. pp. 667-675.

Yahya, N., Puspitasari, P. and Latiff, N. R. A. (2013). Hardness improvement of dental amalgam using zinc oxide and aluminum oxide nanoparticles. In: Ochsner, A., Silva, L. F. M. and Altenbach, H., eds. *Characterization and Development of Biosystems and Biomaterials*. Berlin Heidelberg: Springer-Verlag. pp. 20-21.

Internet Website:

Hardy, S. (2004). Growing lemons in Australia- a production manual. *Lemons Growing Manual*. [online] Available at: http://www.dpi.nsw.gov.au/__data/assets/pdf_file/0016/148120/5b-lemon-rootstocks.pdf [Accessed 17 July 2016].

APPENDICES

Appendix A

Crystalline size of synthesized ZnO NPs

Calculation for β

$$\begin{aligned}\beta &= \frac{\text{FWHM in } 2\theta \times \pi}{180^\circ} \\ &= \frac{0.51420 \times \pi}{180^\circ} \\ &= 8.97 \times 10^{-3}\end{aligned}$$

Calculation for crystalline size by Debye-Scherrer Equation

$$\begin{aligned}D &= \frac{k\lambda}{\beta \cos\theta} \\ &= \frac{(0.9) \times (1.5406 \times 10^{-10} \text{ m})}{(8.97 \times 10^{-3}) \cos(36.2847)} \\ &= 19.22 \text{ nm}\end{aligned}$$

where,

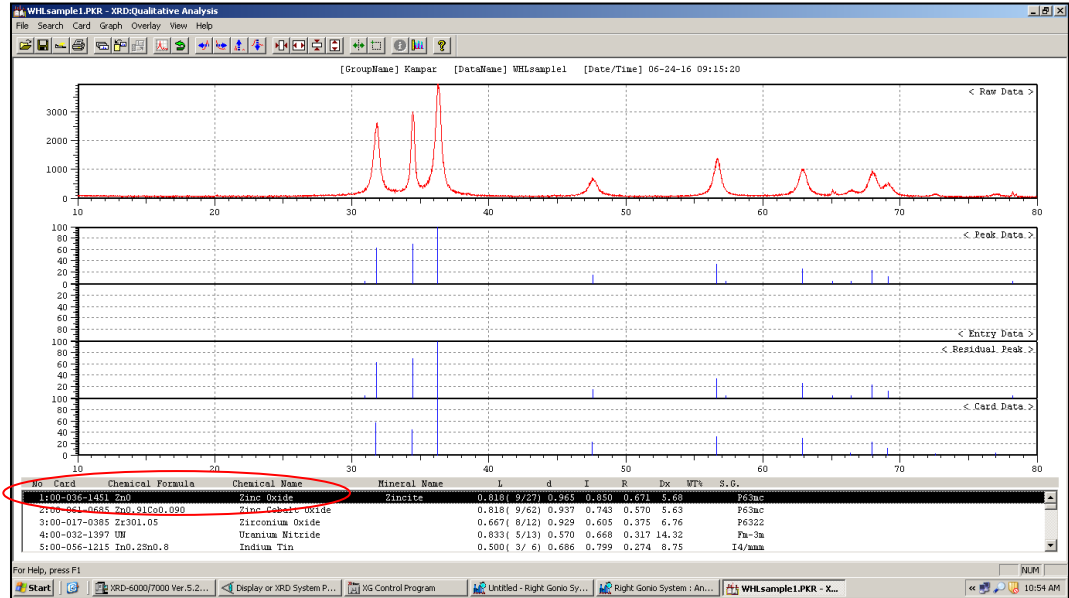
k = Scherrer' constant (usually 0.9)

λ = Wavelength of X-Ray source, Cu K α radiation (1.5406Å)

β = Full width at half-maximum (FWHM) of the diffraction peak in radian

θ = Bragg's diffraction angle

Appendix B



JCPDS Card No. 36-1451 (Diffraction peaks: 31.78°, 34.43°, 36.28°, 47.57°, 56.62°, 62.86°, 67.97° and 69.12°)

Figure: Comparison spectrum between synthesized ZnO NPs with standard card

Appendix C

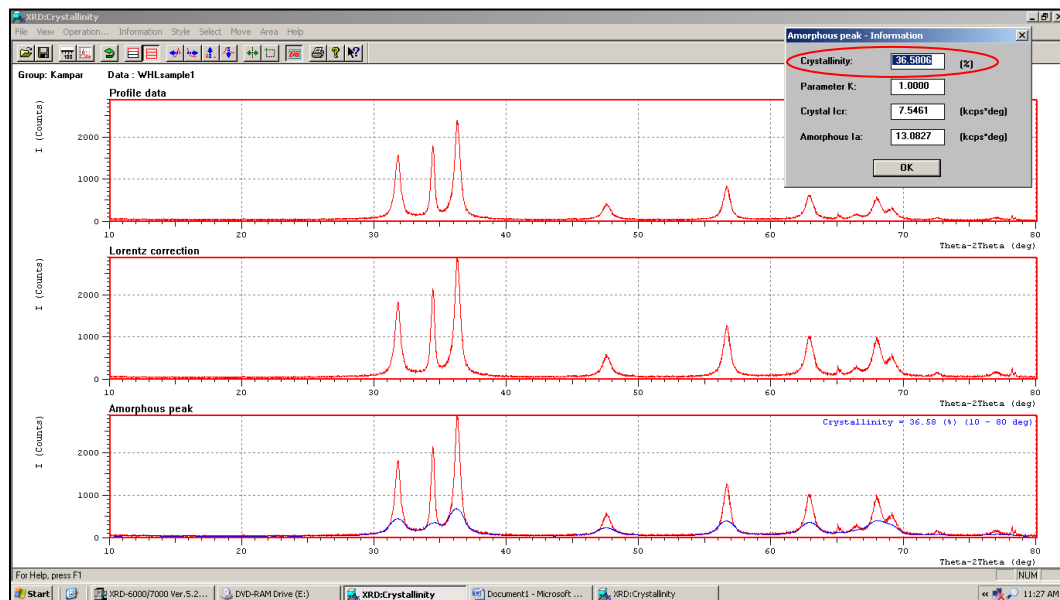


Figure: Crystallinity of synthesized ZnO NPs

Appendix D

```
*** Basic Data Process ***

# Data Information
  Group           : Kampar
  Data            : WHLsample1
  Sample Name    : WHLsample1
  Comment        :
  Date & Time    : 06-24-16 09:15:20

# Measurement Condition
  X-ray tube
    target        : Cu
    voltage       : 40.0 (kV)
    current       : 30.0 (mA)
  Slits
    Auto Slit     : not Used
    divergence slit : 1.00000 (deg)
    scatter slit  : 1.00000 (deg)
    receiving slit : 0.30000 (mm)
  Scanning
    drive axis    : Theta-2Theta
    scan range    : 10.0000 - 80.0000 (deg)
    scan mode     : Continuous Scan
    scan speed    : 2.0000 (deg/min)
    sampling pitch : 0.0200 (deg)
    preset time   : 0.60 (sec)

# Data Process Condition
  Smoothing [ AUTO ]
    smoothing points : 27
  B.G.Subtraction [ AUTO ]
    sampling points : 29
    repeat times    : 30
  Kal-a2 Separate [ MANUAL ]
    Kal a2 ratio    : 50 (%)
  Peak Search [ AUTO ]
    differential points : 27
    FWHM threshold    : 0.050 (deg)
    intensity threshold : 30 (par mil)
    FWHM ratio (n-1)/n : 2
  System error Correction [ NO ]
  Precise peak Correction [ NO ]
```

Figure: Information for XRD analysis (I)

Appendix E

```

*** Basic Data Process ***

Group      : Kampar
Data       : WHLsample1

# Strongest 3 peaks
no. peak   2Theta      d      I/I1    FWHM      Intensity  Integrated Int
           (deg)      (Å)    (deg)   (deg)     (Counts)  (Counts)
1         4      36.2847    2.47383  100    0.51420    1493    49670
2         3      34.4314    2.60263   69    0.36670    1031    23130
3         2      31.7801    2.81345   63    0.51810     942    28280

# Peak Data List
peak      2Theta      d      I/I1    FWHM      Intensity  Integrated Int
no.       (deg)      (Å)    (deg)   (deg)     (Counts)  (Counts)
1         30.9400    2.88790    3    0.37000     47     2296
2         31.7801    2.81345   63    0.51810     942    28280
3         34.4314    2.60263   69    0.36670    1031    23130
4         36.2847    2.47383  100    0.51420    1493    49670
5         47.5680    1.91004   15    0.73600     228    10760
6         56.6212    1.62425   34    0.58020     515    16970
7         57.3200    1.60609    4    0.36000     58     2108
8         62.8637    1.47713   25    0.65090     371    15056
9         65.0833    1.43202    4    0.30000     53      821
10        66.4150    1.40650    4    0.63000     61     2471
11        67.9693    1.37807   22    0.72320     326    12884
12        69.1200    1.35791   11    0.55340     165     6450
13        78.2283    1.22102    3    0.31000     49     1003

```

Figure: Information for XRD analysis (II)

Appendix F

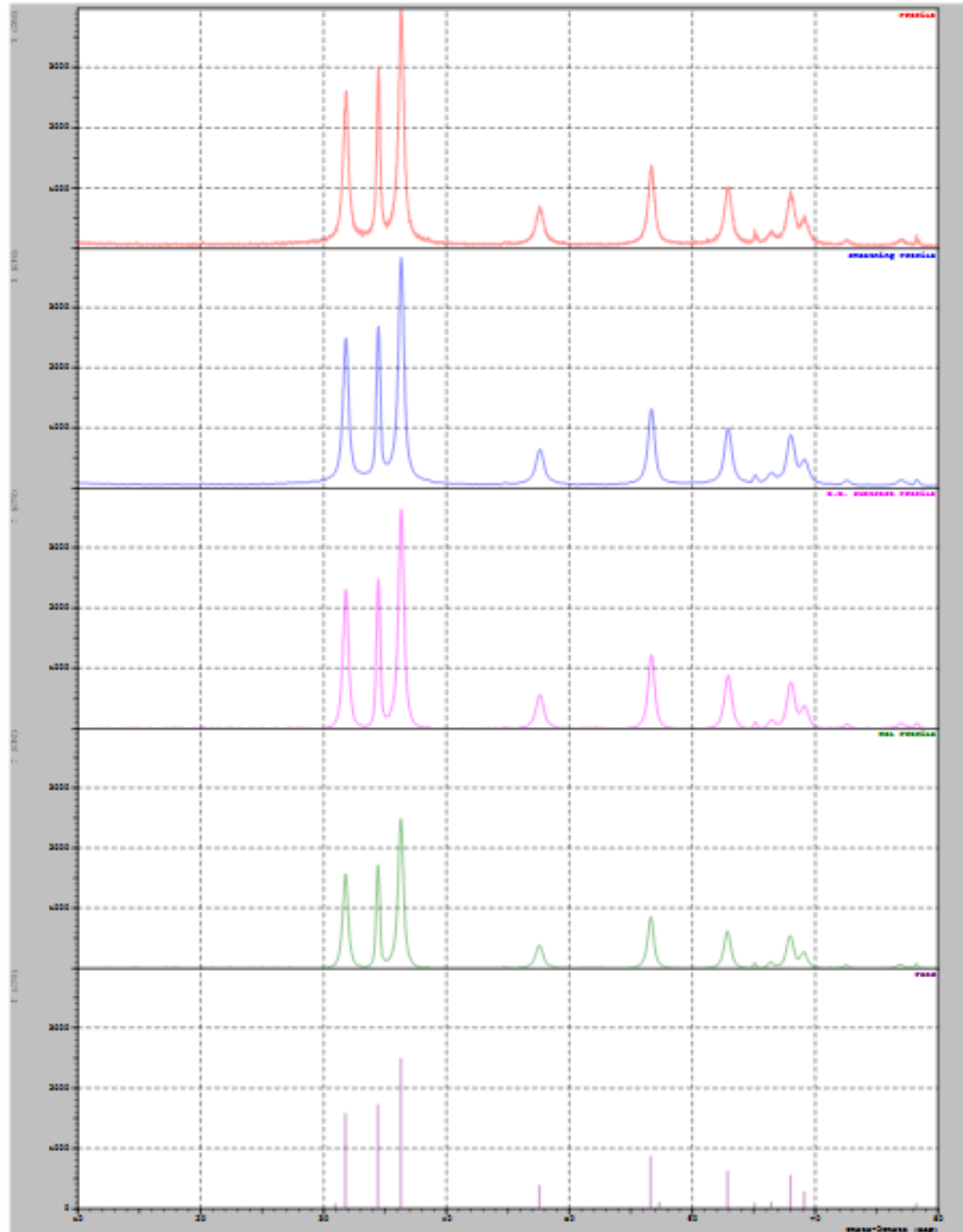


Figure: Information for XRD analysis (III)

Appendix G

Calculation for band gap energy, E_{bg}

$$\begin{aligned} E_{bg} &= \frac{hc}{\lambda} \\ &= \frac{(6.63 \times 10^{-34} \text{ m}^2 \text{ kg s}^{-1}) \times (3.0 \times 10^8 \text{ m s}^{-2})}{(360 \text{ nm})} \\ &= 5.525 \times 10^{-19} \times 6.242 \times 10^{18} \text{ eV} \\ &= 3.45 \text{ eV} \end{aligned}$$

where,

h = Planck's constant ($6.63 \times 10^{-34} \text{ m}^2 \text{ kg s}^{-1}$)

c = Speed of light ($3.00 \times 10^8 \text{ m s}^{-1}$)

λ = Absorption wavelength in UV region (360 nm)

Appendix H

$$\% \text{ Dye Degradation} = \frac{A_0 - A_i}{A_0} \times 100\%$$

where,

A_0 = Initial absorbance of dye solutions

A_i = Absorbance of dye solutions after photocatalytic degradation

Photodegradation CR Dye

Table: Degradation Percentage of CR dye as a function of contact time

Contact Time (mins)	Initial Absorbance	Final Absorbance	Degradation Percentage (%)
0	0.4063	0.4063	0
5	0.4063	0.2920	28.13
10	0.4063	0.1773	56.36
20	0.4063	0.1150	71.70
30	0.4063	0.1078	73.47
40	0.4063	0.0825	79.69
50	0.4063	0.0735	81.91
60	0.4063	0.0680	83.26

Appendix I

Photodegradation of MG Dye

Table: Degradation Percentage of MG dye as a function of contact time

Contact Time (mins)	Initial Absorbance	Final Absorbance	Degradation Percentage (%)
0	1.5690	1.5690	0
10	1.5690	0.4980	68.26
20	1.5690	0.4220	73.10
30	1.5690	0.2350	85.02
60	1.5690	0.1760	88.78
90	1.5690	0.1430	90.89
150	1.5690	0.0730	95.35
210	1.5690	0.0310	98.02